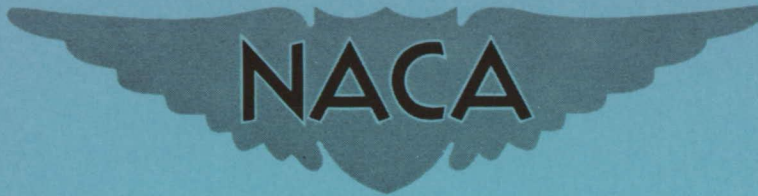


CONFIDENTIAL

277  
Copy  
RM L54A11



# RESEARCH MEMORANDUM

DISTRIBUTION OF LIFT AND PITCHING MOMENT BETWEEN  
WING AND FUSELAGE AND EFFECTS OF WING FLEXIBILITY AND  
DIVE BRAKE ON A 1/30-SCALE SEMISPAN MODEL OF THE  
BELL X-5 AIRPLANE AT TRANSONIC SPEEDS AS  
DETERMINED BY THE NACA WING-FLOW METHOD

By Garland J. Morris and Norman S. Silsby

Langley Aeronautical Laboratory  
Langley Field, Va.

CLASSIFICATION CHANGED TO UNCLASSIFIED

AUTHORITY: NACA RESEARCH ABSTRACT NO. 97

CLASSIFIED DOCUMENT  
DATE: FEBRUARY 24, 1956

This material contains information affecting the National Defense of the United States within the meaning of the espionage laws, Title 18, U.S.C., Secs. 793 and 794, the transmission or revelation of which in any manner to an unauthorized person is prohibited by law.

WHL

NATIONAL ADVISORY COMMITTEE  
FOR AERONAUTICS

WASHINGTON

March 23, 1954

CONFIDENTIAL

## NATIONAL ADVISORY COMMITTEE FOR AERONAUTICS

## RESEARCH MEMORANDUM

DISTRIBUTION OF LIFT AND PITCHING MOMENT BETWEEN  
WING AND FUSELAGE AND EFFECTS OF WING FLEXIBILITY AND  
DIVE BRAKE ON A 1/30-SCALE SEMISPAN MODEL OF THE  
BELL X-5 AIRPLANE AT TRANSONIC SPEEDS AS  
DETERMINED BY THE NACA WING-FLOW METHOD

By Garland J. Morris and Norman S. Silsby

## SUMMARY

An investigation has been made at transonic speeds by the NACA wing-flow method to determine the interaction effects between the wing and fuselage, the effects of wing flexibility, and the effect of the addition of a dive brake on a 1/30-scale semispan model of the Bell X-5 airplane. Lift, pitching moments, and wing bending moments were obtained at various angles of attack for the 60°, 40°, and 20° sweptback duralumin wings in the presence of, but detached from, the fuselage. In addition, lift, drag, and pitching moments were obtained for the complete wing-body-tail configuration with a 60° sweptback wood wing for comparison with the stiffer dural wing, and with a fuselage dive brake on the model with the 60° dural wing. The Reynolds number of the tests was of the order of  $1.0 \times 10^6$ .

Over the Mach number range tested (0.7 to 1.05) the proportion of total lift carried over on the fuselage was, generally, about equal to the ratio of area in the fuselage to the total wing area.

At the lower Mach numbers of the tests there appeared to be little contribution to the longitudinal stability due to the interference effect of the wing on the fuselage at any sweep angle. With the 20° and 40° sweptback wings at the higher Mach numbers the interference apparently produced a stabilizing effect on the fuselage which at a Mach number of 1.0 approximately offset the unstable contribution of the isolated fuselage. With the 60° sweptback wing the net effect of the fuselage was destabilizing up to a Mach number of at least 0.975.

The effect of increasing the flexibility of the 60° sweptback wing in bending by about  $2\frac{1}{2}$  times was a small reduction in lift-curve slope

throughout the test Mach number range. The increased flexibility also would cause a forward shift in aerodynamic center of 4 to 5 percent of the mean aerodynamic chord at lift coefficients from 0 to 0.4 for all Mach numbers covered in these tests, with a dynamic pressure of 545 pounds per square foot.

Addition of the dive brake caused an increment in drag coefficient at zero lift ranging from 0.025 to 0.032 over the Mach number range tested but appeared to have little effect on drag due to lift. The effect of the dive brake on the pitching moment was principally a nose-down increment of 0.02 to 0.045, depending on Mach number. There appeared to be little or no effect on longitudinal stability. A reduction in lift-curve slope of about 8 percent resulted from application of the dive brakes at Mach numbers up to 0.90.

## INTRODUCTION

As part of a program to determine the aerodynamic characteristics of the Bell X-5 airplane incorporating a wing whose angle of sweep can be varied in flight, an investigation has been made at transonic speeds by the NACA wing-flow method on a 1/30-scale semispan model. The semispan model tested differed in some details from the full-scale aircraft. Results of tests at a Mach number of 1.24 have been reported in references 1 to 5. Results of tests at transonic speeds of the effects of sweepback on the longitudinal-control effectiveness and downwash characteristics are reported in references 6 and 7.

Presented herein are results of tests made to determine the distribution of lift and pitching moment between the fuselage and wings swept back  $20^\circ$ ,  $40^\circ$ , and  $60^\circ$ , and the root bending moment of the  $40^\circ$  and  $60^\circ$  sweptback wings. In addition the effect of wing flexibility and the effect of a flap-type fuselage dive brake on the longitudinal characteristics of the model with the wing swept back  $60^\circ$  were determined. Results are in terms of lift and drag coefficients, pitching moment, and wing bending-moment coefficients for the various configurations over a range of angles of attack. The effective Mach number at the wing of the model covered a range from about 0.7 to 1.05 and the Reynolds number was of the order of  $1.0 \times 10^6$ .

## SYMBOLS

- B wing bending moment about streamwise axis through wing pivot point, in-lb
- b/2 model wing span, in.

$b_{1/2}$	span from pivot point to model wing tip, in.
$c$	local wing chord parallel to plane of symmetry, in.
$\bar{c}$	mean aerodynamic chord of wing, based on the relationship $\frac{\int_0^{b/2} c^2 dy}{\int_0^{b/2} c dy}, \text{ in.}$
$\bar{c}_t$	mean aerodynamic chord of tail, in.
$C_B$	bending-moment coefficient, $B/qS_e \frac{b_1}{2}$
$C_D$	drag coefficient, $D/qS$
$C_{DF}$	drag coefficient of fuselage, based on wing area
$C_L$	lift coefficient, $L/qS$ , or $L/qS_e$ where indicated
$C_m$	pitching-moment coefficient, $M/qS\bar{c}$
$C_N$	normal-force coefficient, based on exposed wing area, $N/qS_e$
$D$	drag, lb
$i_t$	incidence of horizontal tail, referred to wing chord plane, deg
$L$	lift, lb
$M$	pitching moment about center line of balance, in-lb
$M_L$	local Mach number at wing surface of North American F-51D airplane
$M_w$	effective Mach number for wing of model
$N$	normal force, lb
$q$	effective dynamic pressure for wing of model, lb/sq ft
$R_w$	Reynolds number based on mean aerodynamic chord of wing $\bar{c}$
$R_t$	Reynolds number based on mean aerodynamic chord of tail $\bar{c}_t$

- S wing area of semispan model (area within fuselage is considered to be formed by perpendiculars to the plane of symmetry from the leading and trailing edge of the wing at the wing-fuselage intersection),  $\int_0^{b/2} c \, dy$ , sq ft
- $S_e$  exposed wing area of semispan model, sq ft
- $y$  spanwise coordinate, in.
- $\bar{y}$  lateral center-of-pressure location from pivot point,  

$$\left( \frac{C_B - C_{B(C_N=0)}}{C_N} \right) \frac{b_1}{2}, \text{ in.}$$
- $\alpha$  angle of attack, referred to wing chord plane, deg
- $\Lambda$  sweepback angle referred to 25-percent-chord line of wing swept back  $50^\circ$ , deg

A prime indicates coefficients based on dimensions of configuration with  $60^\circ$  sweptback wing.

#### APPARATUS AND TESTS

The tests were made by the NACA wing-flow method, in which the model is mounted in a region of high-speed flow over the wing of a North American F-51D airplane. The modified contour of the F-51D airplane wing in the test region for the present investigation (the same as that used for the tests of refs. 6 and 7) gave a nearly uniform velocity field at local Mach numbers through the transonic speed range.

The 1/30-scale semispan model of the Bell X-5 airplane consisted of various combinations of a fuselage with end plate attached, three duralumin wings swept back  $20^\circ$ ,  $40^\circ$ , and  $60^\circ$ , a  $60^\circ$  sweptback wood wing with a steel core, a horizontal tail of  $0^\circ$  and  $-2^\circ$  incidence angle, and a flap-type dive brake. The wood wing and the  $60^\circ$  sweptback dural wing had the same dimensions. The geometric characteristics of the model are given in table I and figure 1.

In tests to determine the distribution of aerodynamic forces between the wing and fuselage, the dural wings were separated from the fuselage by a small gap to allow for the measurement of forces on the wing in the presence of the fuselage. A small end plate was attached to the wing

root at the wing-fuselage juncture and was spaced from the fuselage by about 0.02 inch to minimize the leakage of air through the gap between the wing and fuselage (see figs. 2 and 3). No horizontal tail was installed for these wing-detached tests. The wing shank, which passed through the test surface of the F-51D airplane wing, was equipped with strain gages to measure bending moments on the model wing in the presence of the fuselage.

In a test to determine the effect of the wing end plate and the gap between the wing and fuselage in the wing-detached tests, the 60° swept-back wing with end plate was attached to the fuselage, still retaining the gap between the fuselage and end plate.

The 60° sweptback wood wing, which was built of laminated birch glued to a thin steel core (see fig. 4), was tested in combination with the fuselage and a horizontal tail of 0° incidence (fig. 5) in order to indicate the effect of flexibility on the aerodynamic characteristics of the model.

The dimensions and location of the brake are shown in figure 6 and a photograph of the configuration is shown in figure 7.

The model was designed and constructed so that the pitching moment would be measured about the gross-weight center-of-gravity location of the full-scale airplane. This center-of-gravity location originally corresponded to the 25-percent mean-aerodynamic-chord position of the wing in each sweep position. However, some changes in the design of the full-scale airplane, specifically, a reduction in wing span and the addition of a trailing-edge fillet to the wings in all sweep positions except 60°, were incorporated in the semispan model before its construction was completed; these changes altered the mean aerodynamic chords and their locations so that now 26 percent of the mean aerodynamic chord of the 60° sweptback wing and 35 percent of the mean aerodynamic chord of the 40° and 20° sweptback wings correspond to the center-of-gravity position about which the pitching moments were taken. Still later changes in the airplane, not incorporated in the semispan model of the present tests, have altered both the trailing-edge fillets and the longitudinal location of the wings with respect to the fuselage; that is, the translational locations of the wing-pivot point for the various sweep angles of the model do not correspond with those of the full-scale Bell X-5. The mean aerodynamic chords and their relations to the pivot points are different because of the trailing-edge fillets on the model.

The mounting of the model and the method of testing were similar to that described in references 6 and 7. Because the model and balance were arranged to oscillate as a unit, forces were measured normal and parallel to the fuselage reference line of the model at all angles of attack. Continuous measurements were made of angle of attack, normal force, chord

force, and pitching moment as the model was oscillated at a rate of about  $20^\circ$  per second through an angle-of-attack range of about  $-4^\circ$  to  $12^\circ$ .

The chordwise Mach number distributions in the test region on the airplane wing, as determined from static pressure measurements at the wing surface with the model removed, are shown in figure 8. The method of determining the effective dynamic pressure  $q$  at the model wing and the effective Mach number  $M_w$  at the model wing can be found in references 6 and 7.

The variation of Reynolds number of the  $60^\circ$  sweptback wing and the horizontal tail with Mach number is indicated in figure 9. The Reynolds number of the other wings may be obtained by multiplying the Reynolds number of the  $60^\circ$  sweptback wing by the ratio of the mean aerodynamic chords.

In order to facilitate reference to the various test configurations, the following abbreviated designations have been adopted:

#### Wing-Detached Configurations

<u>Designation</u>	<u>Description of Configuration</u>
$\begin{pmatrix} W_{\Lambda d}^{Feg} \\ W_{20d}^{Feg} \\ W_{40d}^{Feg} \\ W_{60d}^{Feg} \end{pmatrix}$	$20^\circ$ , $40^\circ$ , and $60^\circ$ sweptback dural wings in the presence of, but detached d from, the fuselage; small end plate e attached to the root of the wing with a gap g of about 0.02 inch from the fuselage; no horizontal tail.

#### Wing-Attached Configurations

<u>Designation</u>	<u>Description of Configurations</u>
$W_{\Lambda}^F$	dural wing-fuselage configuration of reference 7
$W_{60}^{Feg}$	$60^\circ$ sweptback dural wing-fuselage configuration with wing end plate e; gap g around fuselage of configurations $W_{\Lambda d}^{Feg}$ approximately simulated; no horizontal tail.
$W_{w60}^{FT_0}$	$60^\circ$ sweptback wood w wing-fuselage configuration with horizontal tail; $i_t = 0^\circ$
$W_{60}^{FT_0}$	$60^\circ$ sweptback dural wing-fuselage configuration with horizontal tail; $i_t = 0^\circ$ (ref. 7)

$W_{60}^{FbrT-2}$	60° sweptback dural wing-fuselage configuration equipped with dive brake and horizontal tail; $i_t = -2^\circ$
$W_{60}^{FT-2}$	60° sweptback dural wing-fuselage configuration with horizontal tail; $i_t = -2^\circ$ (ref. 6)

## Other Configurations

F fuselage-alone configuration of reference 6

## PRESENTATION OF RESULTS

The results are presented in figures 10 to 21. The following table lists the quantities and configurations shown and the figures in which they appear:

Quantity	Configurations	Figure
Sample data	$W_{60d}^{Feg}$	10
$C_m'$ and $\alpha$ against $M_w$ for various $C_L'$	$W_{60d}^{Feg}$	11(a)
$C_m$ and $\alpha$ against $M_w$ for various $C_L$	$W_{40d}^{Feg}$	11(b)
	$W_{20d}^{Feg}$	11(c)
$C_m'$ and $\alpha$ against $M_w$ for various $C_L'$	$W_{60}^{Feg}$	12
$C_L'$ against $\alpha$ for various $M_w$	$W_{60}^F$ (ref. 7); $W_{60d}^{Feg}$ ; $W_{60}^{Feg}$	13(a)
$C_L$ against $\alpha$ for various $M_w$	$W_{40}^F$ (ref. 7); $W_{40d}^{Feg}$	13(b)
	$W_{20}^F$ (ref. 7); $W_{20d}^{Feg}$	13(c)
$C_m'$ against $\alpha$ for various $M_w$	$W_{60d}^{Feg}$ ; F (ref. 6); $W_{60}^{Feg}$ ; $W_{60}^F$ (ref. 7)	14(a)

Quantity	Configurations	Figure
$C_m$ against $\alpha$ for various $M_w$	$W_{40d}^{Feg}$ ; $W_{40}^F$ (ref. 7); $F$ (ref. 6)	14(b)
	$W_{20d}^{Feg}$ ; $W_{20}^F$ (ref. 7); $F$ (ref. 6)	14(c)
$C_B'$ and $C_B$ against $M_w$ for various $C_N$	$W_{60d}^{Feg}$ ; $W_{40d}^{Feg}$	15
$\frac{\bar{y}}{b_{l/2}}$ against $C_L$ for various $M_w$	$W_{60d}^{Feg}$ ; $W_{40d}^{Feg}$	16
Center-of-pressure location on wing panel for various $C_L$ and $M_w$	$W_{60d}^{Feg}$ ; $W_{40d}^{Feg}$	17
$C_m'$ , $C_D'$ , and $\alpha$ against $M_w$ for various $C_L'$	$W_{w60}^{FT0}$	18
$C_L'$ against $\alpha$ $C_L'$ against $C_L'$ $C_L'$ against $C_D'$	for various $M_w$ $W_{w60}^{FT0}$ ; $W_{60}^{FT0}$ (ref. 7)	19(a)
		19(b)
		19(c)
$C_m'$ , $C_D'$ , and $\alpha$ against $M_w$ for various $C_L'$	$W_{60}^{FbrT-2}$	20
$C_L'$ against $C_D'$ $C_L'$ against $\alpha$ $C_m'$ against $C_L'$	for various $M_w$ $W_{60}^{FbrT-2}$ ; $W_{60}^{FT-2}$ (ref. 6)	21(a)
		21(b)
		21(c)

## DISCUSSION

Sample data are shown in figure 10 for one oscillation through the angle-of-attack range. The Mach number  $M_w$  varied from 0.798 to 0.782 during the cycle. The curves faired through the points are taken to apply to the average Mach number of 0.79 for the cycle. Similarly, data from several cycles were reduced for each configuration and cross-plotted to show variations of the characteristics with Mach number at constant

lift coefficients (e.g., see fig. 11). The curves showing the variations of the coefficients with Mach number are presented as basic data and are cross-plotted at specific Mach numbers for discussion (e.g., fig. 13).

All pitching-moment results are referred to the fuselage station on the model corresponding to the gross-weight center-of-gravity fuselage station of the full-scale airplane; this station corresponds to 26 percent of the mean aerodynamic chord for the 60° sweptback wing, and 35 percent of the mean aerodynamic chord for the 40° and 20° sweptback wings.

Because of excessive vibration in the record of bending moment during the test of configuration  $W_{20d}^{F_{eg}}$ , the bending-moment data were not worked up for this configuration; hence the bending-moment coefficient  $C_B$  and the spanwise center-of-pressure location  $\frac{\bar{y}}{b_1/2}$  are missing in figures 15 and 16, respectively, for this configuration.

No force corrections have been made for the small Mach number gradient except that the gradient over the model wing area has been integrated to obtain the effective Mach number of the model wing  $M_w$ .

#### Distribution of Lift Between Wing and Fuselage

In figure 13 the lift coefficients for the  $W_{\Delta d}^{F_{eg}}$  configurations are based on exposed wing area, whereas those for the  $W_{\Delta}^F$  configurations are based on total wing area including the area of the fuselage (see table I and fig. 1). With the 60° sweptback wing the slopes of the lift curves were quite similar for the two conditions throughout the Mach number range covered, indicating that the proportion of lift carried over on the fuselage was about equal to the ratio of the area within the fuselage to the total wing area. A similar result was obtained for the configuration with 40° sweepback except that for Mach numbers above about 0.8 the lift carried by the fuselage appeared to be slightly greater. With 20° sweepback the proportion of lift carried by the fuselage generally tended to be somewhat less than the ratio of the areas.

#### Pitching-Moment Distribution Between Wing and Fuselage

A comparison of the variation of pitching-moment coefficient with angle of attack for configuration  $W_{60}^{F_{eg}}$  and  $W_{60}^F$  (fig. 14(a)) indicates that, over the Mach number range tested, the gap and end plate at the wing-fuselage junction of the  $W_{60}^{F_{eg}}$  configuration increased the nose-down pitching moment at zero angle of attack only slightly (0.005 or less), increased the stability slightly at angles of attack up to

$3^\circ$  or  $4^\circ$ , and decreased it somewhat at higher angles. Whether these effects arise from changes in flow over the fuselage or over the wing was not determined and therefore the contributions of the wing interference on the fuselage to the stability, as indicated by comparisons of the pitching-moment data for configurations  $W_{\Delta d}F_{eg}$ ,  $W_{\Delta}F$ , and  $F$  should be considered as qualitative.

With the  $60^\circ$  sweptback-wing configuration, it was found that by adding the pitching-moment coefficients for the  $F$  configuration to those for the  $W_{60d}F_{eg}$  condition (fig. 14), curves of  $C_M$  against  $\alpha$  were obtained (not shown) which conformed quite closely to the curves shown for the  $W_{60}F$  or  $W_{60}F_{eg}$  case for all Mach numbers covered in the tests (up to 0.975 for this sweep angle). This result indicates that the fuselage in the presence of the wing produced essentially the same destabilizing effect as the isolated fuselage; that is, there was little or no contribution to the longitudinal stability from the interaction effect of the wing on the fuselage. Similar results were obtained with the  $20^\circ$  and  $40^\circ$  sweep angles at Mach numbers up to about 0.90. With further increase in Mach number, the presence of the wing apparently reduced the unstable contribution of the fuselage so that at a Mach number of 1.0 the forces acting on the fuselage had little or no net effect on the stability. From the results presented in reference 5 it was found that with the  $60^\circ$  sweptback wing also, at higher Mach numbers (1.24), the unstable moment variation of the isolated fuselage was largely offset by the presence of the wing.

#### Center of Pressure of Wing

With  $60^\circ$  sweep, the lateral location of the center of pressure of the semispan wing at all Mach numbers tested moved outboard from about 40 percent to between 50 percent and 55 percent of the exposed semispan (measured perpendicular to the fuselage center line) as the lift coefficient was increased from 0 to about 0.4 (fig. 16). A study of pitching-moment data indicated that the location of the center of pressure moved approximately along the sweep lines (fig. 17). At higher lift coefficients (0.5 to 0.6) the center of pressure tended to return inboard and to move slightly to the rear. There appeared to be little variation of the lateral center of pressure with Mach number at the highest test lift coefficients; however, at the lower lift coefficients the center of pressure generally moved outboard perpendicular to the free stream with increasing Mach number up to a Mach number of 0.9, after which it returned part way inboard.

With the wing swept back  $40^\circ$  there was relatively little variation in the center-of-pressure position with lift coefficient below a  $C_L$  of 0.4 for Mach numbers up to 0.9. At higher lift coefficients in this

Mach number range the center of pressure tended to move inboard, more or less along the sweep line. With Mach numbers above 0.9 an outboard movement of the center of pressure occurred, especially at low lift coefficients. Increasing the Mach number caused the center of pressure to move rearward and also outboard at the high lift coefficients.

### Flexibility

The  $W_{w60FT_0}$  configuration, which had a wood wing about 42 percent as rigid in bending as the  $W_{60FT_0}$  dural wing, showed only a slight reduction in lift-curve slope, as compared with the dural-wing configuration, up to an angle of attack of about  $5^\circ$  (fig. 19(a)). Above  $5^\circ$  the variation of lift with angle of attack was greater than at lower angles of attack but not as great as that shown by the dural-wing configuration. The reduction in lift with increased flexibility results, of course, from a decrease in the local angle of attack along the span for streamwise sections as the swept wing bends.

The reduction of the local angle of attack along the span of a sweptback wing also results in decreased stability (fig. 19(b)). Over the lift-coefficient range from 0 to 0.4, the average location of the aerodynamic center of the wood-wing configuration was about 4.5 percent of the mean aerodynamic chord farther forward than for the dural-wing configuration at a Mach number of 0.75 and about 6.5 percent of the mean aerodynamic chord farther forward at a Mach number of 1.00. For these tests the dynamic pressure increased from 545 to 780 pounds per square foot as the Mach number was increased from 0.7 to 1.0. For a constant dynamic pressure of 545 pounds per square foot the forward shift of the aerodynamic center would be about 4.5 percent of the mean aerodynamic chord throughout the Mach number range covered.

### Effects of Dive Brake

Addition of the dive brake to configuration  $W_{60FT_2}$  resulted in an increment in drag coefficient at zero lift ranging from 0.03 to 0.032 over the Mach number range tested (fig. 21(a)) except at  $M = 1.00$ , where the increment appeared to be about 0.025. The dive brake apparently had little or no effect on the increase in drag coefficient with increasing lift (i.e., on the drag due to lift). The results in reference 4 indicated an increment in drag coefficient due to the same dive brake of 0.046 at a Mach number of 1.24. A reduction in lift-curve slope of about 8 percent was caused by the dive brake in the range of lift coefficient from 0 to 0.3 for Mach numbers up to 0.9. At higher Mach numbers the effect on lift-curve slope appeared to decrease up to a Mach number of 1.0.

From the previous tests at a Mach number of 1.24 it was found that the dive brake reduced the lift-curve slope by about 8 percent for this condition.

The principal effect of the dive brake on the pitching-moment characteristics (fig. 21(c)) was a nose-down change of moment coefficient which varied from 0.025 to 0.045 as the Mach number increased from 0.75 to 0.95. With a further increase in Mach number to 1.0, the difference in moment coefficient decreased again to about 0.025. At a Mach number of 1.24 (ref. 4) the dive brake caused little or no change in trim. The dive brake apparently had practically no effect on longitudinal stability in the range of Mach numbers covered, as evidenced by the parallelism of the curves of figure 21(c). This result was also obtained in the tests at a Mach number of 1.24.

### CONCLUSIONS

The results of an investigation to determine the interaction effects between the wing and fuselage, the effects of wing flexibility, and the effect of the addition of a dive brake on a 1/30-scale semispan model of the Bell X-5 airplane at transonic speeds are as follows:

1. The proportion of total lift carried over on the fuselage was generally about equal to the ratio of wing area within the fuselage to the total wing area over the Mach number range tested (0.75 to 1.05).
2. There was little or no contribution to the longitudinal stability from the interaction effect of the wing on the fuselage throughout the test Mach number range (0.700 to 0.975) for the 60° sweptback wing and at Mach numbers up to about 0.90 for the 20° and 40° sweptback wings. With further increase in Mach number above 0.9, the presence of the wing apparently reduced the unstable contribution of the fuselage on the 20° and 40° sweptback wings until the forces acting on the fuselage had little or no net effect on the stability at a Mach number of 1.0.
3. The effect of increasing the flexibility of the 60° sweptback wing in bending by about  $2\frac{1}{2}$  times was a small reduction in lift-curve slope, especially at the high angles of attack, over the Mach number range tested.

The increased flexibility also caused a forward shift in the aerodynamic center of 4 to 5 percent of the mean aerodynamic chord at lift coefficients from 0 to 0.4 at all test Mach numbers for a dynamic pressure of 545 pounds per square foot.

4. Addition of the dive brake caused an increment in drag coefficient at zero lift varying from 0.025 to 0.032, depending on Mach number, but did not appear to have much effect on drag due to lift. The lift-curve slope was reduced about 8 percent by the dive brake at Mach numbers up to 0.90. The effect of the dive brake on longitudinal stability was small but it resulted in a nose-down pitching-moment-coefficient increment of 0.02 to 0.045, depending on the Mach number.

Langley Aeronautical Laboratory,  
National Advisory Committee for Aeronautics,  
Langley Field, Va., January 7, 1953.

## REFERENCES

1. Silsby, Norman S., Morris, Garland J., and Kennedy, Robert M.: Longitudinal Characteristics at Mach Number of 1.24 of 1/30-Scale Semispan Model of Bell X-5 Variable-Sweep Airplane With Wing Swept Back 60° From Tests by NACA Wing-Flow Method. NACA RM L50E02a, 1950.
2. Morris, Garland J., Kennedy, Robert M., and Silsby, Norman S.: The Effect of Sweepback on the Longitudinal Characteristics at a Mach Number of 1.24 of a 1/30-Scale Semispan Model of the Bell X-5 Airplane From Tests by the NACA Wing-Flow Method. NACA RM L50I28, 1950.
3. Sawyer, Richard H., Kennedy, Robert M., and Morris, Garland J.: Longitudinal-Control Effectiveness and Downwash Characteristics at a Mach Number of 1.24 of a 1/30-Scale Semispan Model of the Bell X-5 Airplane As Determined by the NACA Wing-Flow Method. NACA RM L50K15, 1951.
4. Kennedy, Robert M.: Effects of a Fuselage Flap Dive Brake on the Aerodynamic Characteristics of 1/30-Scale Semispan Model of the Bell X-5 Variable-Sweep Airplane at a Mach Number 1.24 As Determined by the NACA Wing-Flow Method. NACA RM L50L11a, 1951.
5. Silsby, Norman S., and Morris, Garland J.: Investigation of the Distribution of Lift, Drag, and Pitching Moment Between the Wing and Fuselage of a 1/30-Scale Semispan Model of the Bell X-5 Airplane at a Mach Number of 1.24 by the NACA Wing-Flow Method. NACA RM L51K27, 1952.
6. Kolnick, Joseph J., and Kennedy, Robert M.: The Effects of Sweepback on Longitudinal Characteristics of a 1/30-Scale Semispan Model of the Bell X-5 Airplane As Determined From NACA Wing-Flow Tests at Transonic Speeds. NACA RM L52I23, 1952.
7. Silsby, Norman S., and Morris, Garland J.: Longitudinal-Control Effectiveness and Downwash Characteristics at Transonic Speeds of a 1/30-Scale Semispan Model of the Bell X-5 Airplane As Determined by the NACA Wing-Flow Method. NACA RM L52K12, 1953.

TABLE I.- GEOMETRIC CHARACTERISTICS OF 1/30-SCALE  
SEMISPAN MODEL OF BELL X-5 AIRPLANE

Wing dimensions:

Airfoil section (perpendicular to unswept 38.6-percent-chord line)			
Root . . . . .		NACA 64(10)A011	
Tip . . . . .		NACA 64(08)A008.6	
Sweepback angle, deg . . . . .	20	40	60
Semispan, in. . . . .	6.18	5.31	3.88
Mean aerodynamic chord, in. . . . .	2.96	3.10	3.64
Chord at tip, in. . . . .	1.84	1.84	1.84
Chord at plane of symmetry, in. . . . .	4.50	4.40	4.25
Area (semispan), sq in. . . . .	15.84	14.97	13.79
Exposed area, sq in. . . . .	12.38	11.55	10.52
Aspect ratio . . . . .	4.82	3.77	2.18
Dihedral (chord plane), deg . . . . .	0	0	0
Incidence (chord plane), deg . . . . .	0	0	0

Horizontal tail:

Section . . . . .	NACA 64A006		
Semispan, in. . . . .			1.91
Mean aerodynamic chord, in. . . . .			1.43
Chord at tip, in. . . . .			0.72
Chord at plane of symmetry, in. . . . .			1.95
Area (semispan) sq in. . . . .			2.55
Aspect ratio . . . . .			2.86
Height (above wing chord), in. . . . .			0.56
Tail length from 0.26c̄ of 60° wing to 0.25c̄ <sub>t</sub> , in. . . . .			6.83

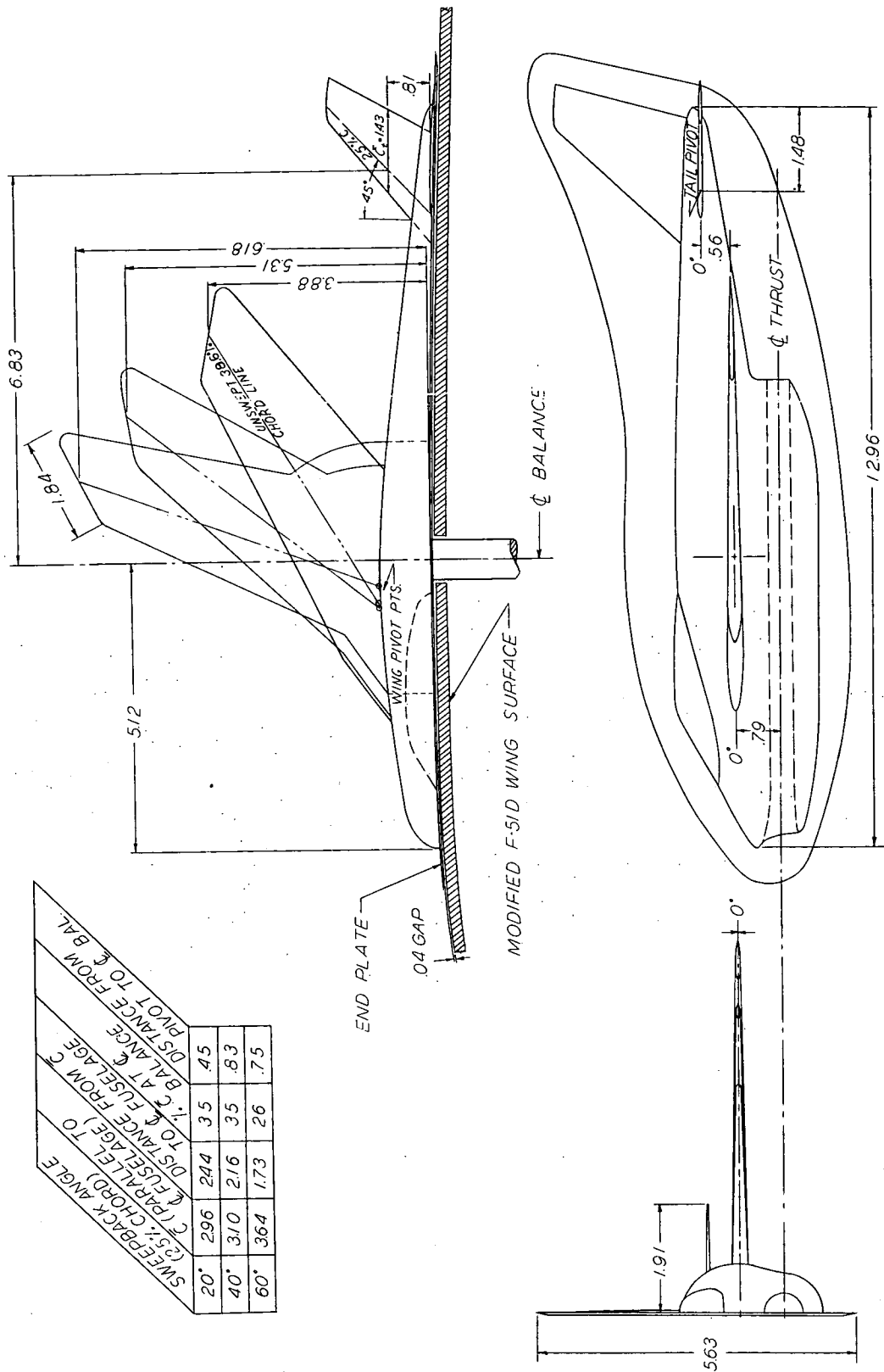


Figure 1.- Details of the semispan model of the Bell X-5 airplane. (All dimensions are in inches.)

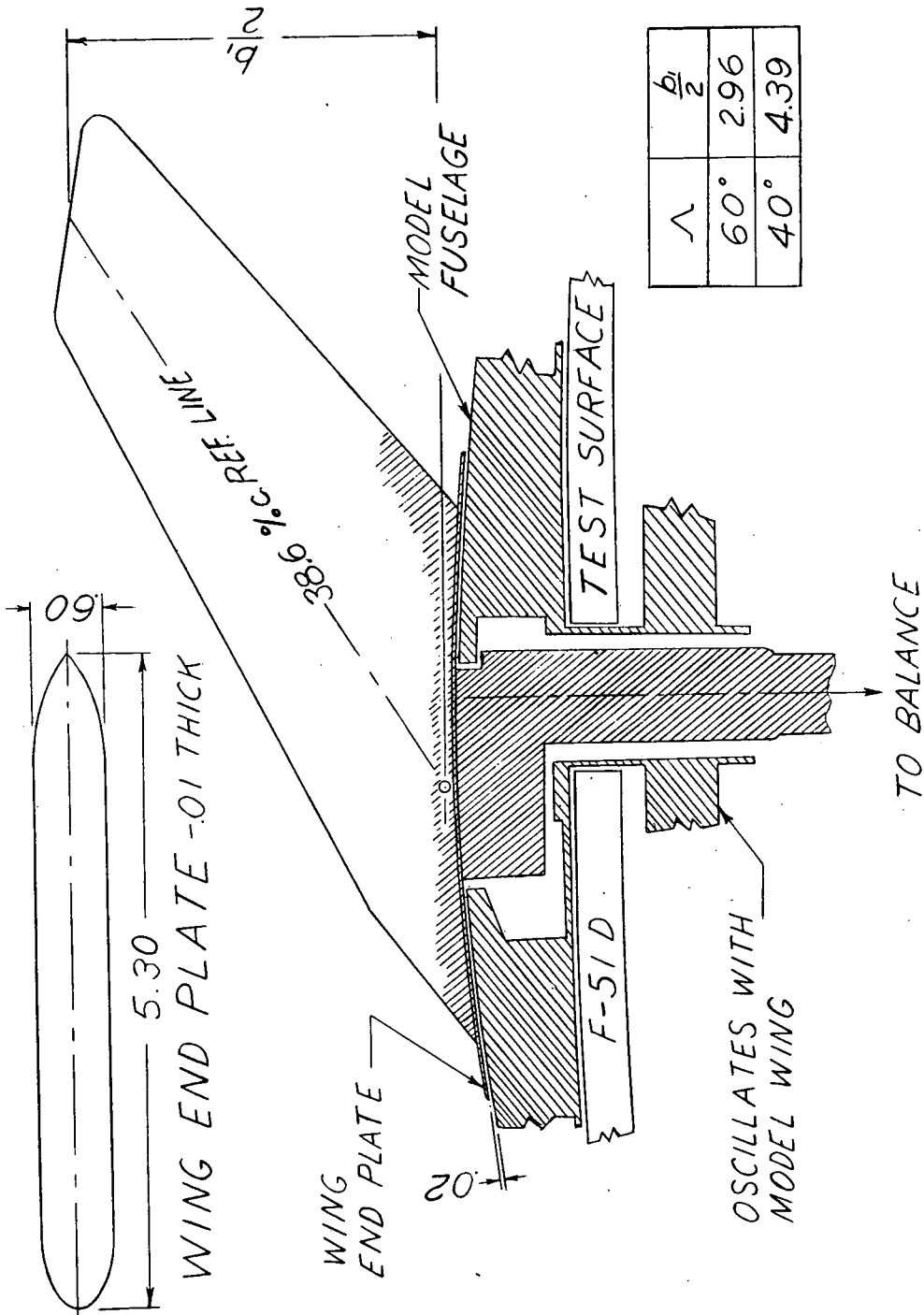
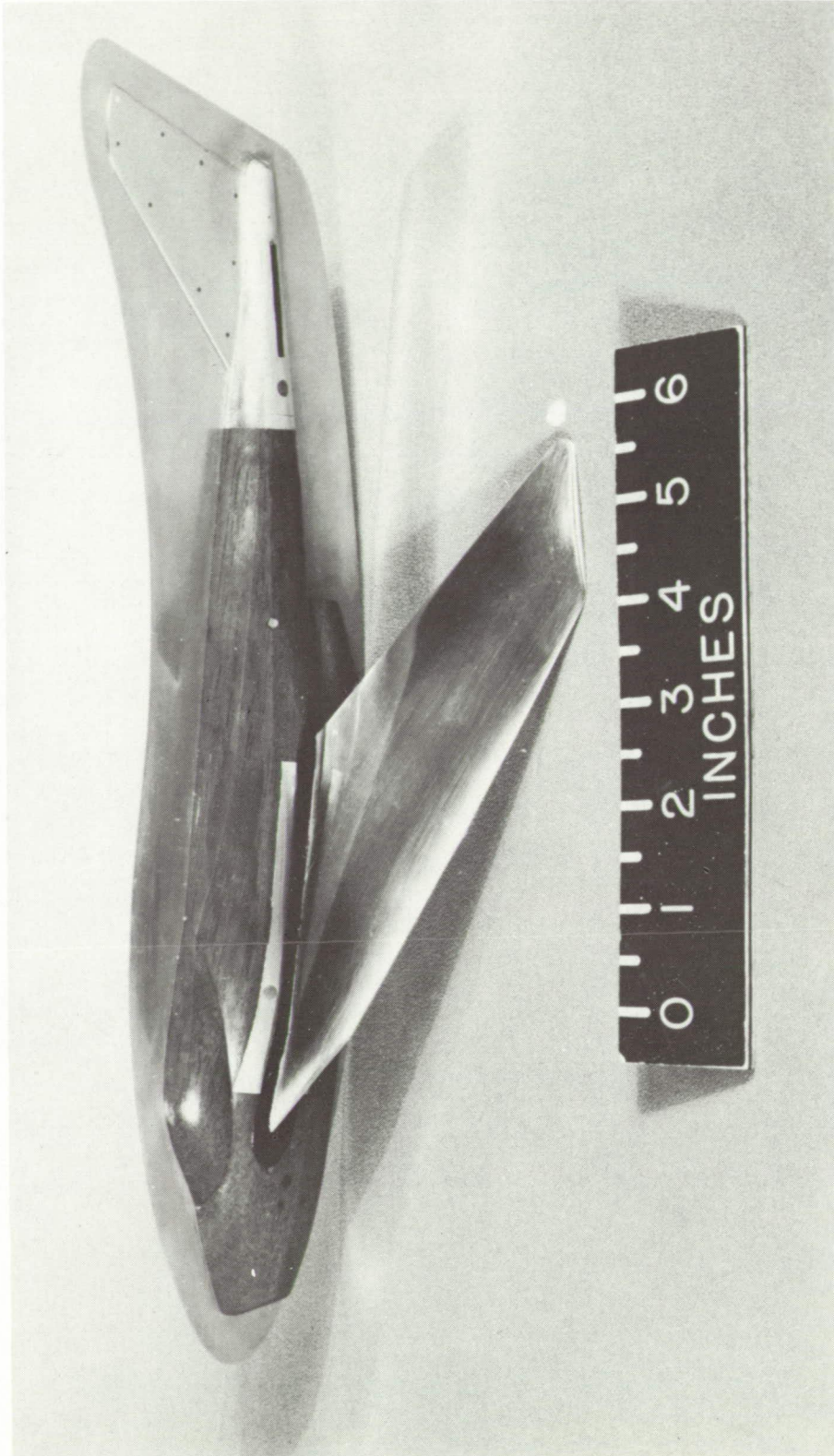


Figure 2.- Schematic diagram of apparatus for testing model wings in presence of, but detached from, model fuselage. (All dimensions are in inches.)



L-67413

Figure 3.- Photograph of 60° sweptback wing with wing-root end plate attached, in presence of, but detached from, fuselage of Bell X-5 wing-flow model.

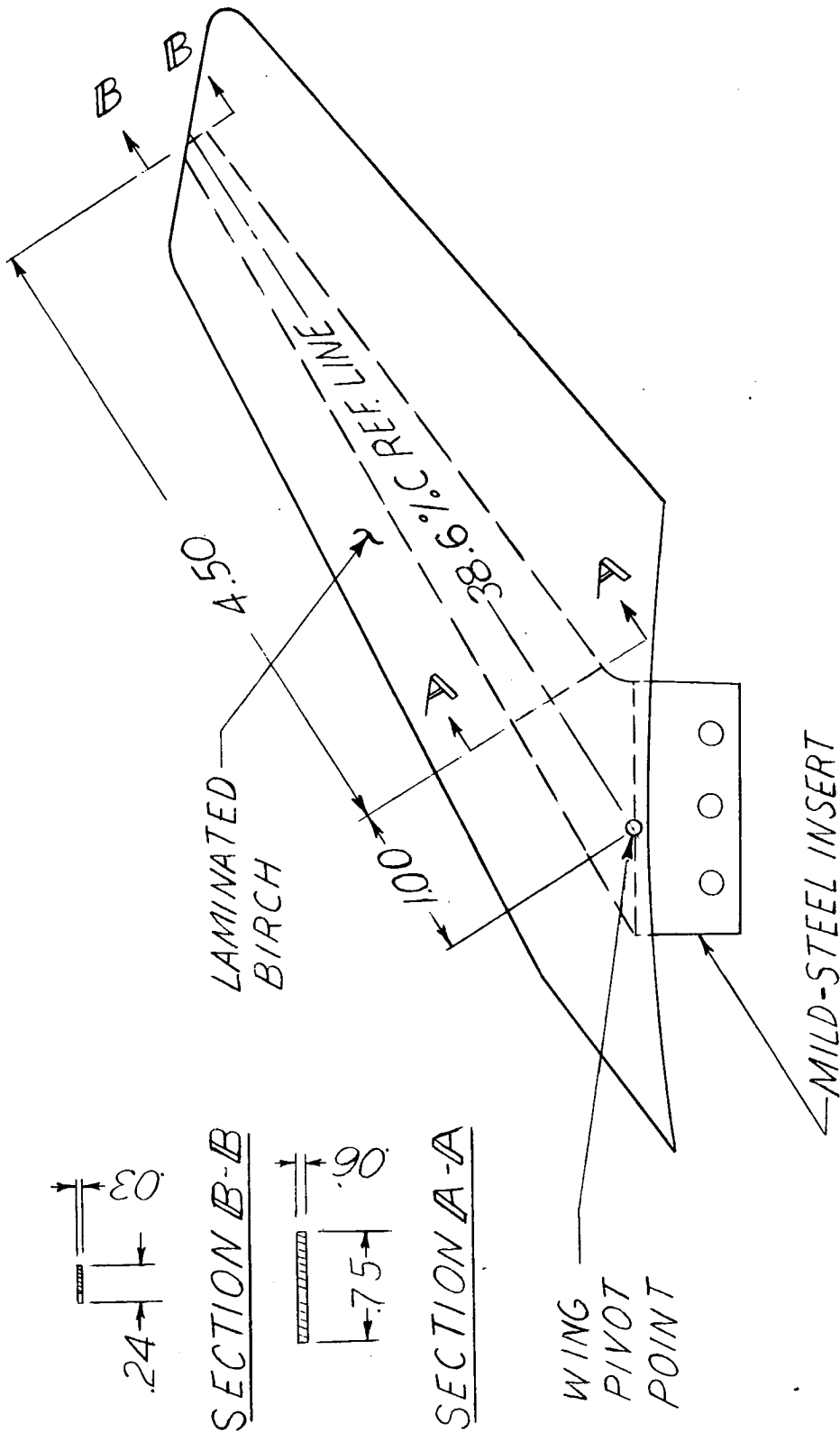
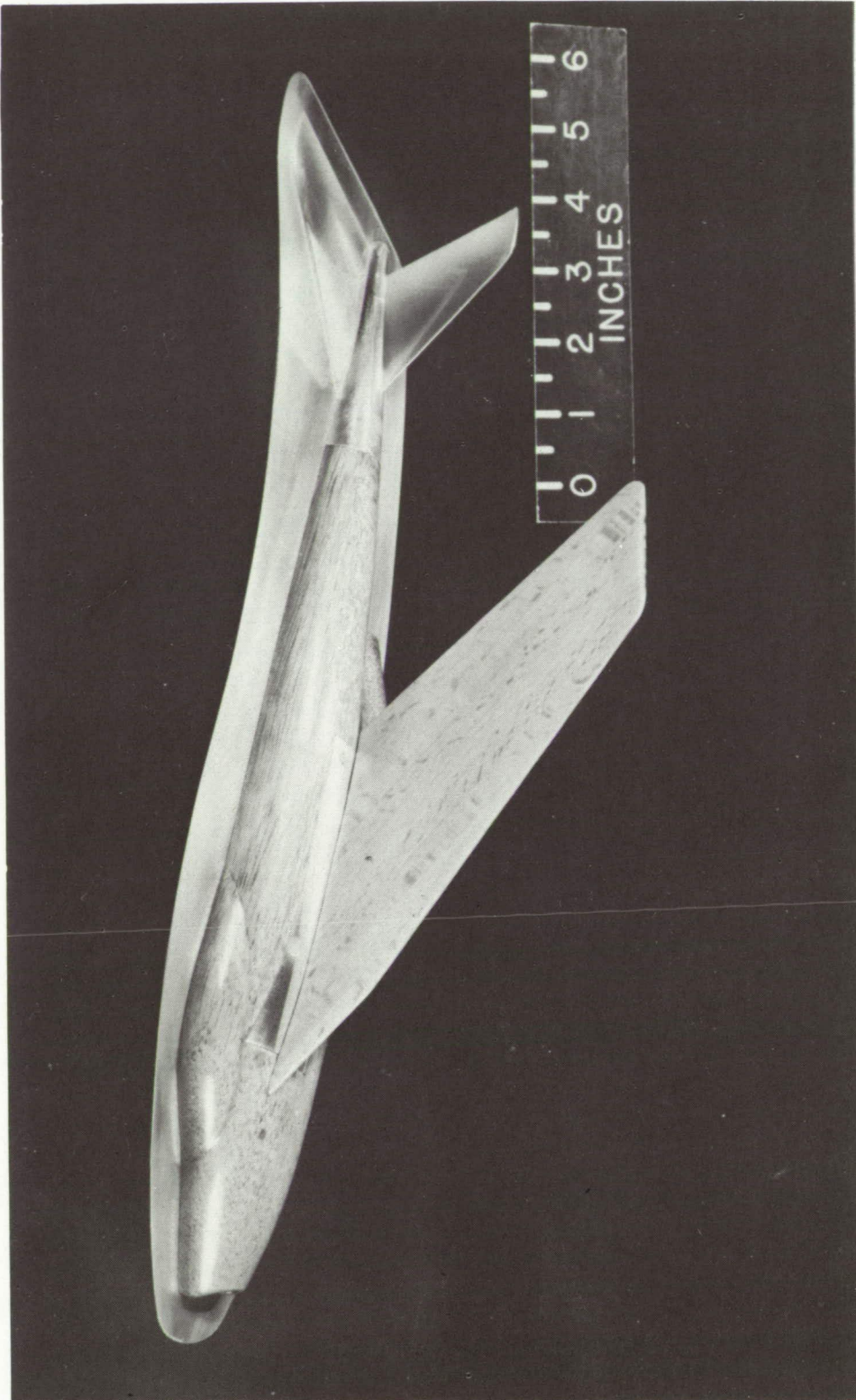


Figure 4.- Details of wood wing. All dimensions are in inches.



L-63079.1

Figure 5.- Photograph of Bell X-5 semispan wing-flow model with 60° swept-back wood wing.

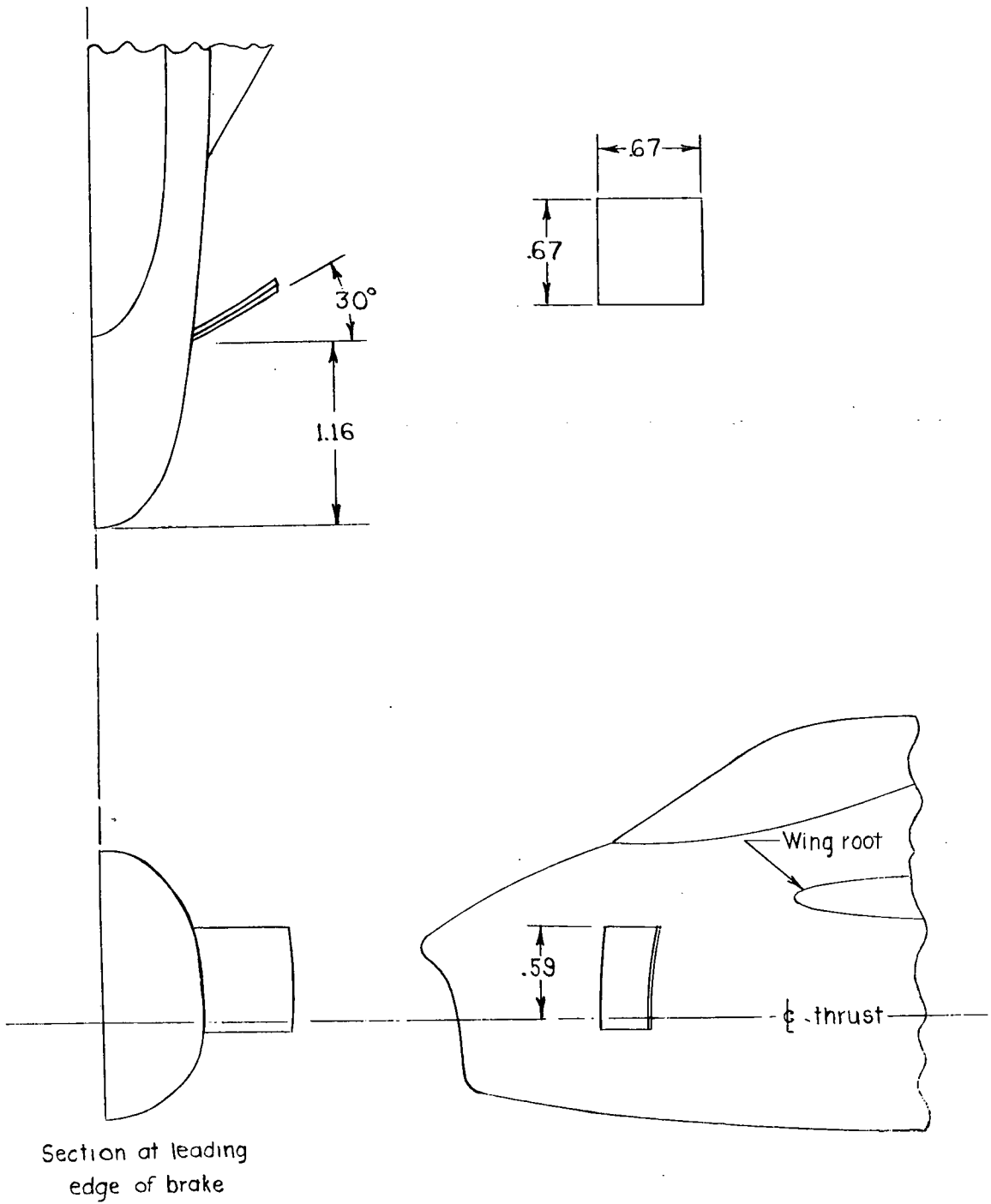
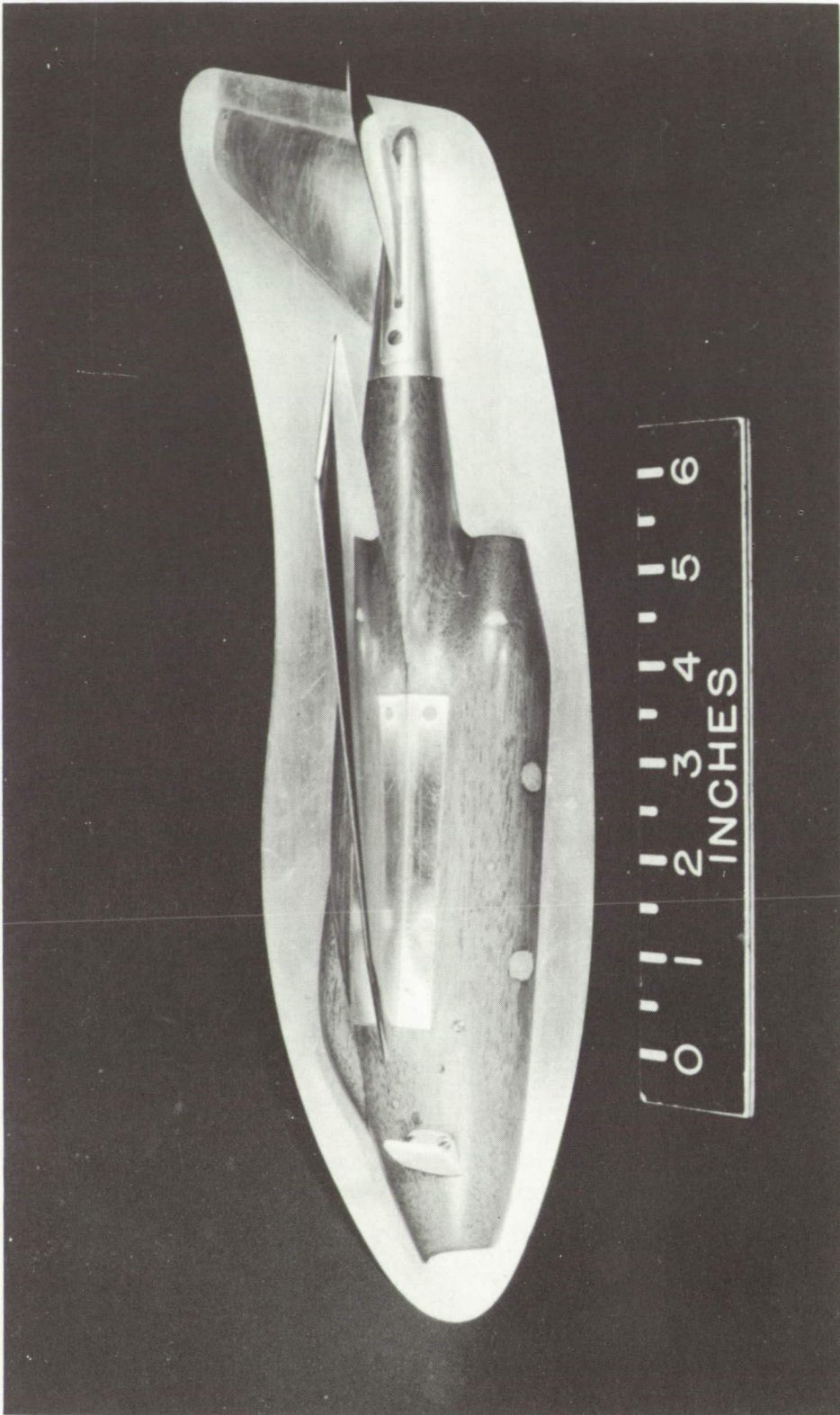


Figure 6.- Fuselage flap dive brake on 1/30-scale Bell X-5 model. All dimensions are in inches.



L-65399

Figure 7.- Side view of semispan wing-flow model of the Bell X-5 airplane with fuselage flap dive brake attached.

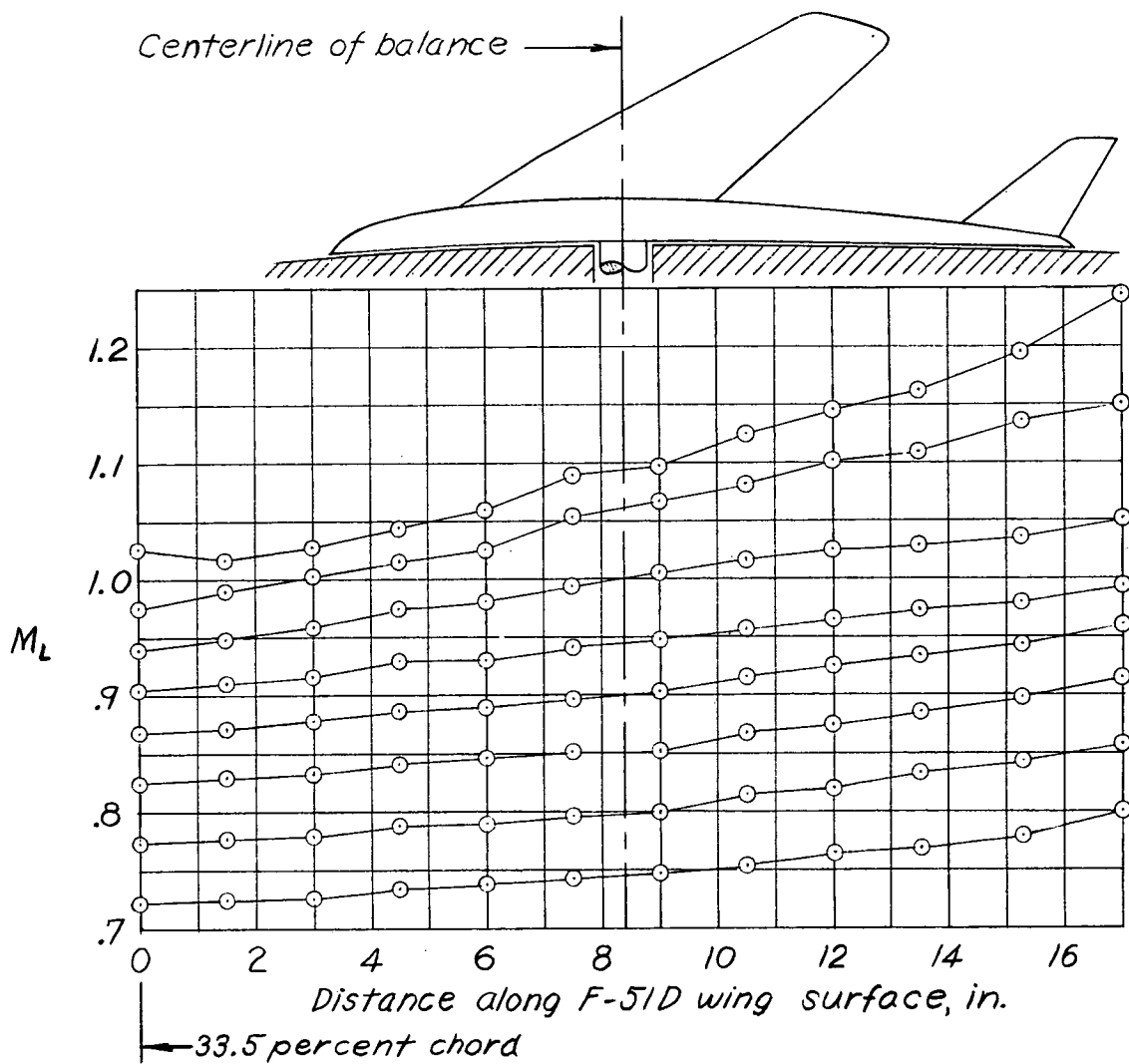


Figure 8.- Typical chordwise local Mach number variation measured at surface of test section. Chordwise location of model also shown.

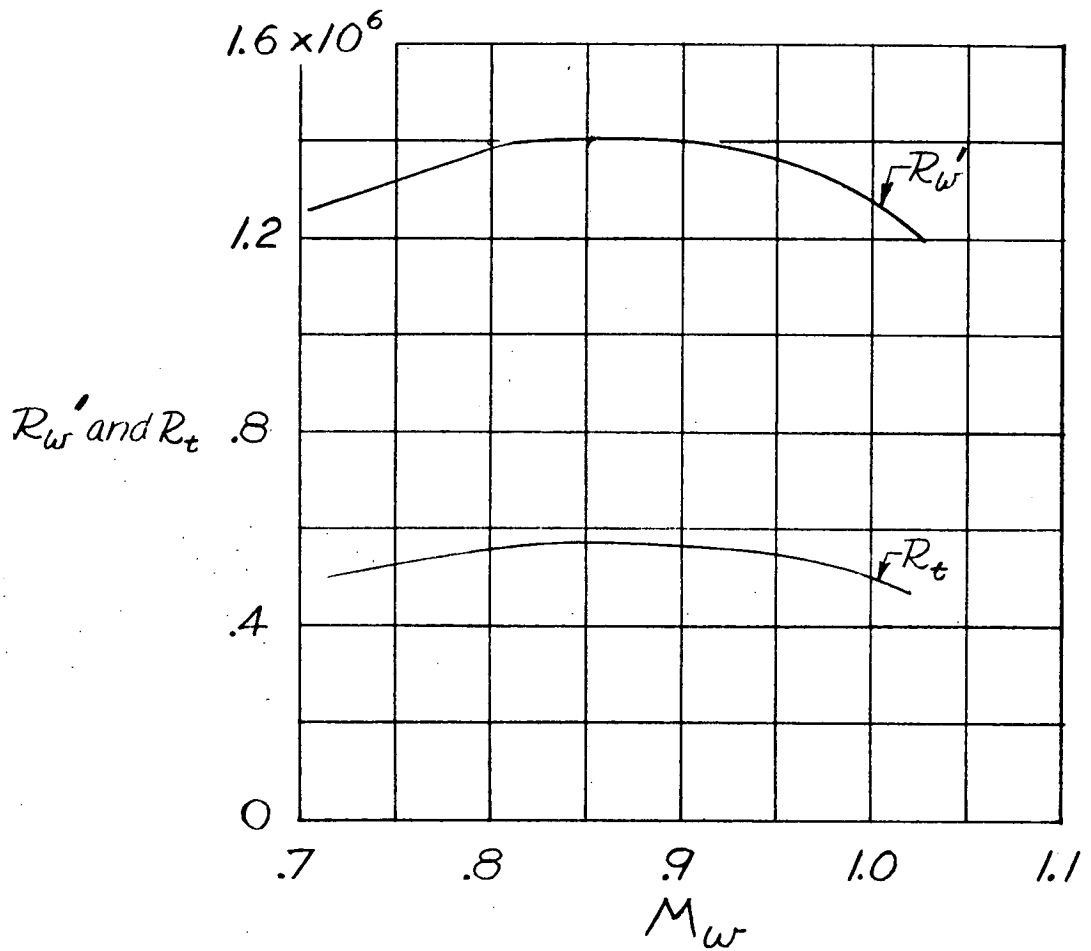


Figure 9.- Variation of Reynolds number of 60° sweptback wing  $R_w'$  and Reynolds number of tail  $R_t$  with Mach number at the wing  $M_w$ .

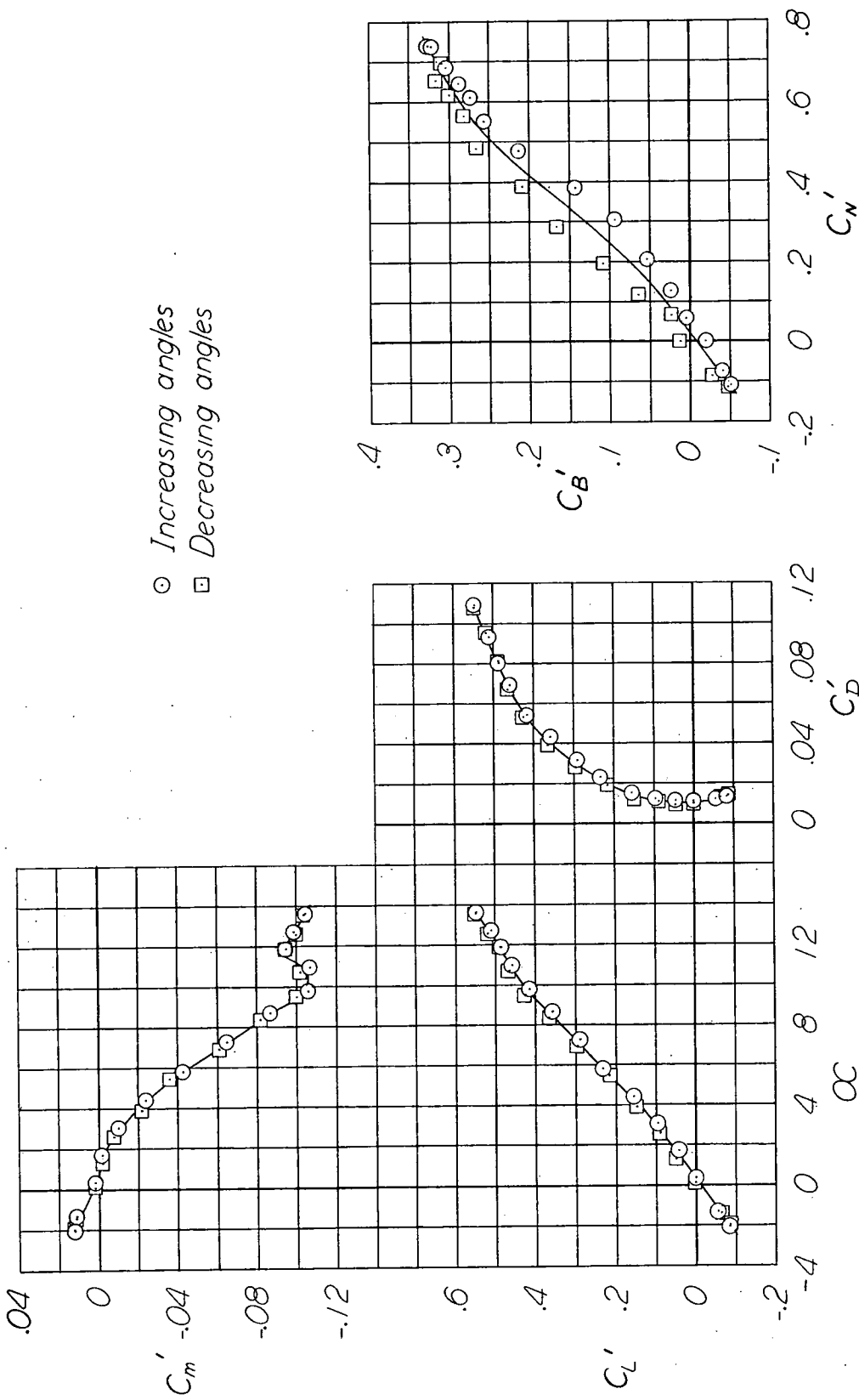
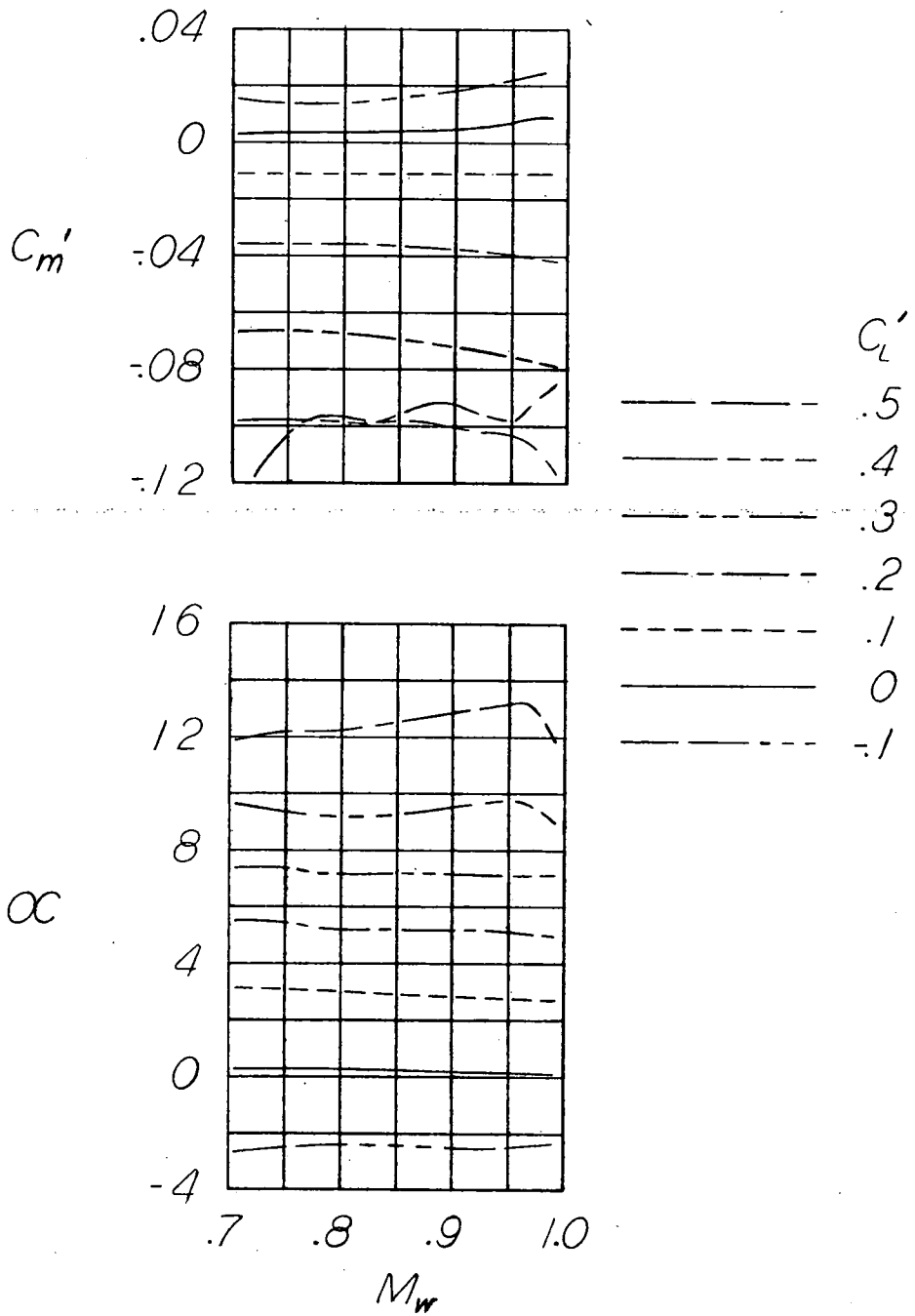
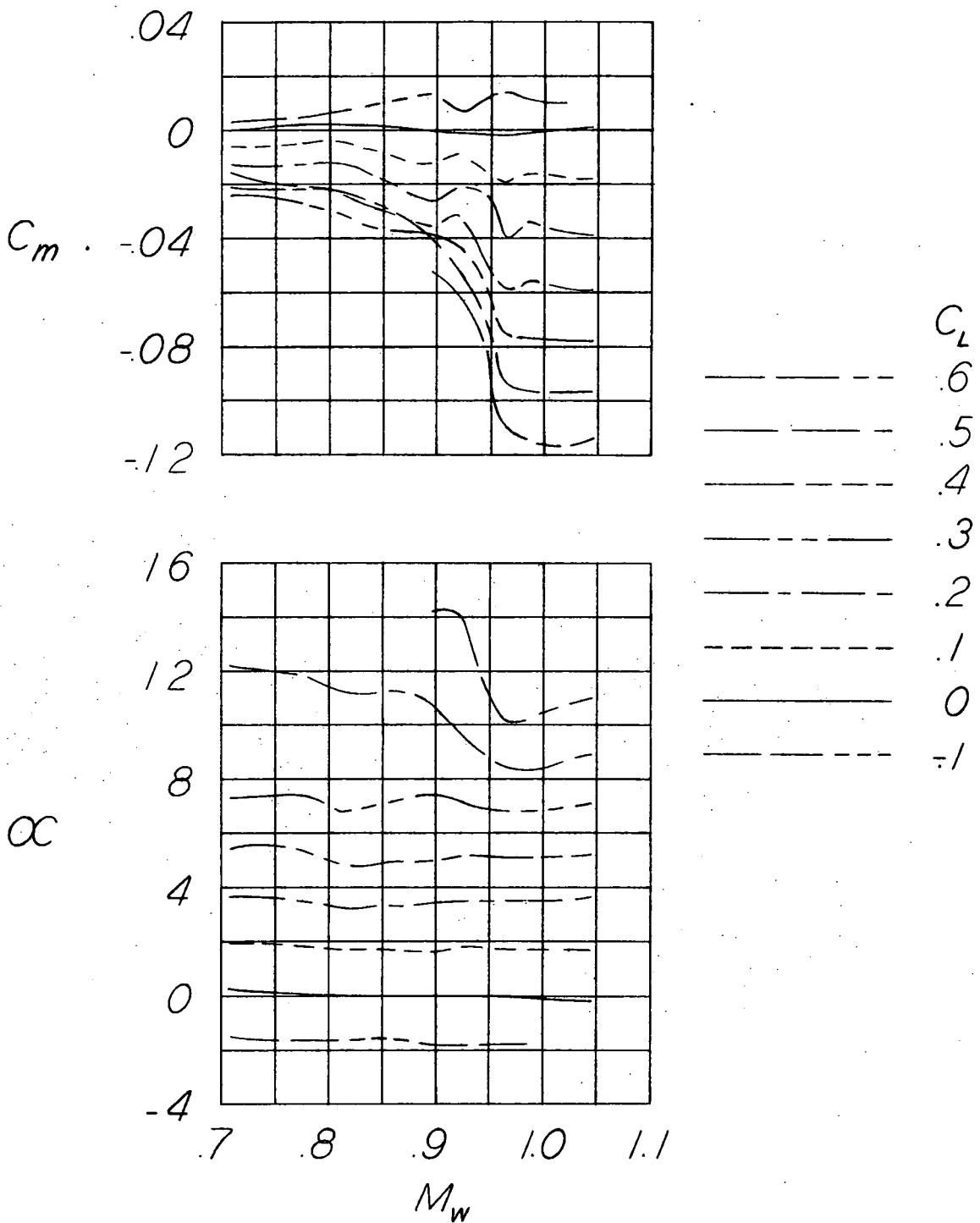


Figure 10.- Sample data for the Bell X-5 semispan airplane model.  
 Configuration W60dFeg;  $M_w = 0.79$ .



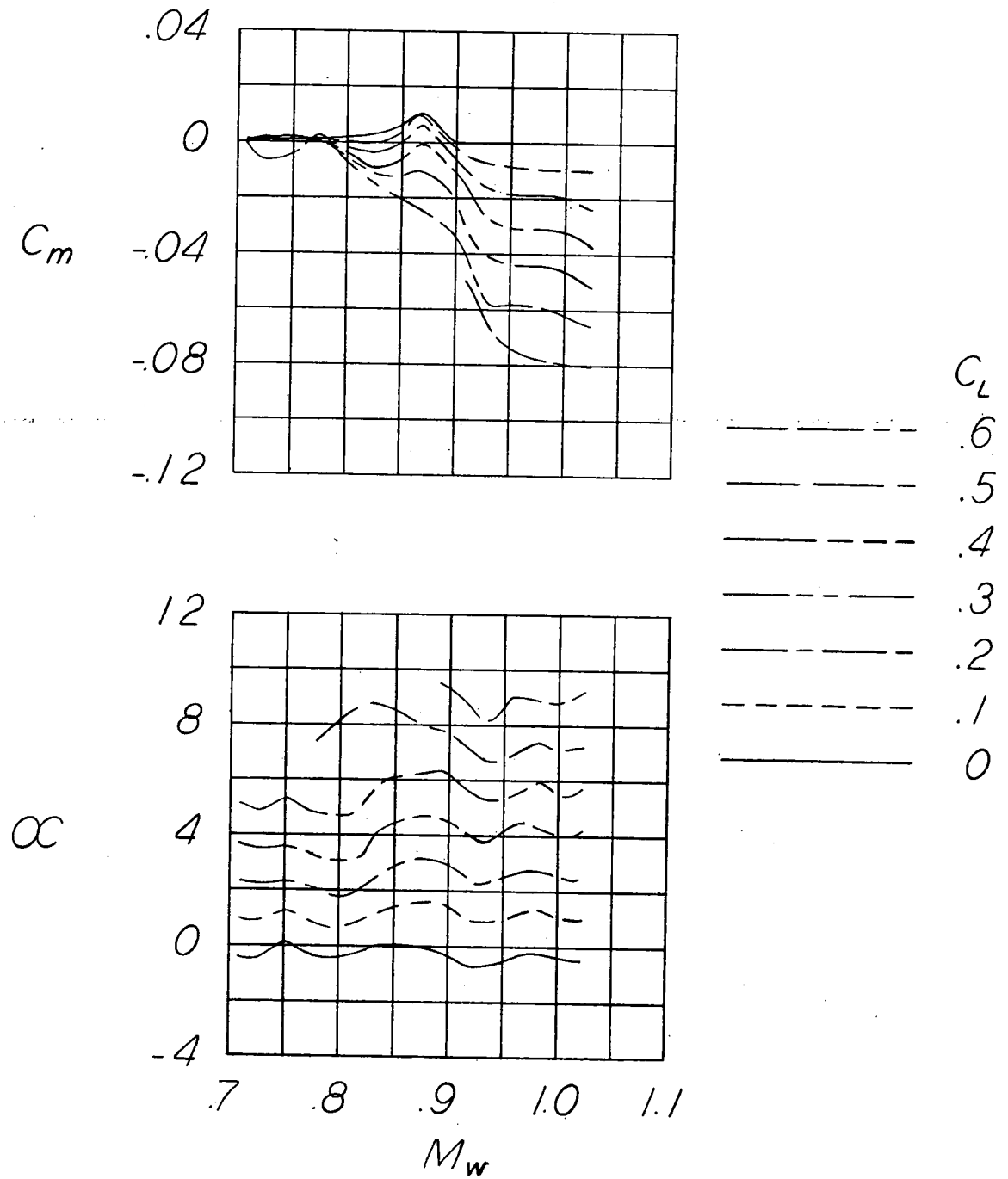
(a)  $\Lambda = 60^\circ$  ( $W_{60dFeg}$ ).

Figure 11.- Variation with Mach number of  $C_m$  and  $\alpha$  at various lift coefficients for wing of semispan wing-flow model of Bell X-5 airplane in presence of, but detached from, model fuselage. Configurations  $W_{AdFeg}$ ; tail off. (Coefficients based on respective wing dimensions.)



(b)  $\Lambda = 40^\circ$  ( $W_{40dF_{eg}}$ ).

Figure 11.- Continued.



(c)  $\Lambda = 20^\circ$  ( $w_{20d}^{F_{eg}}$ ).

Figure 11.- Concluded.

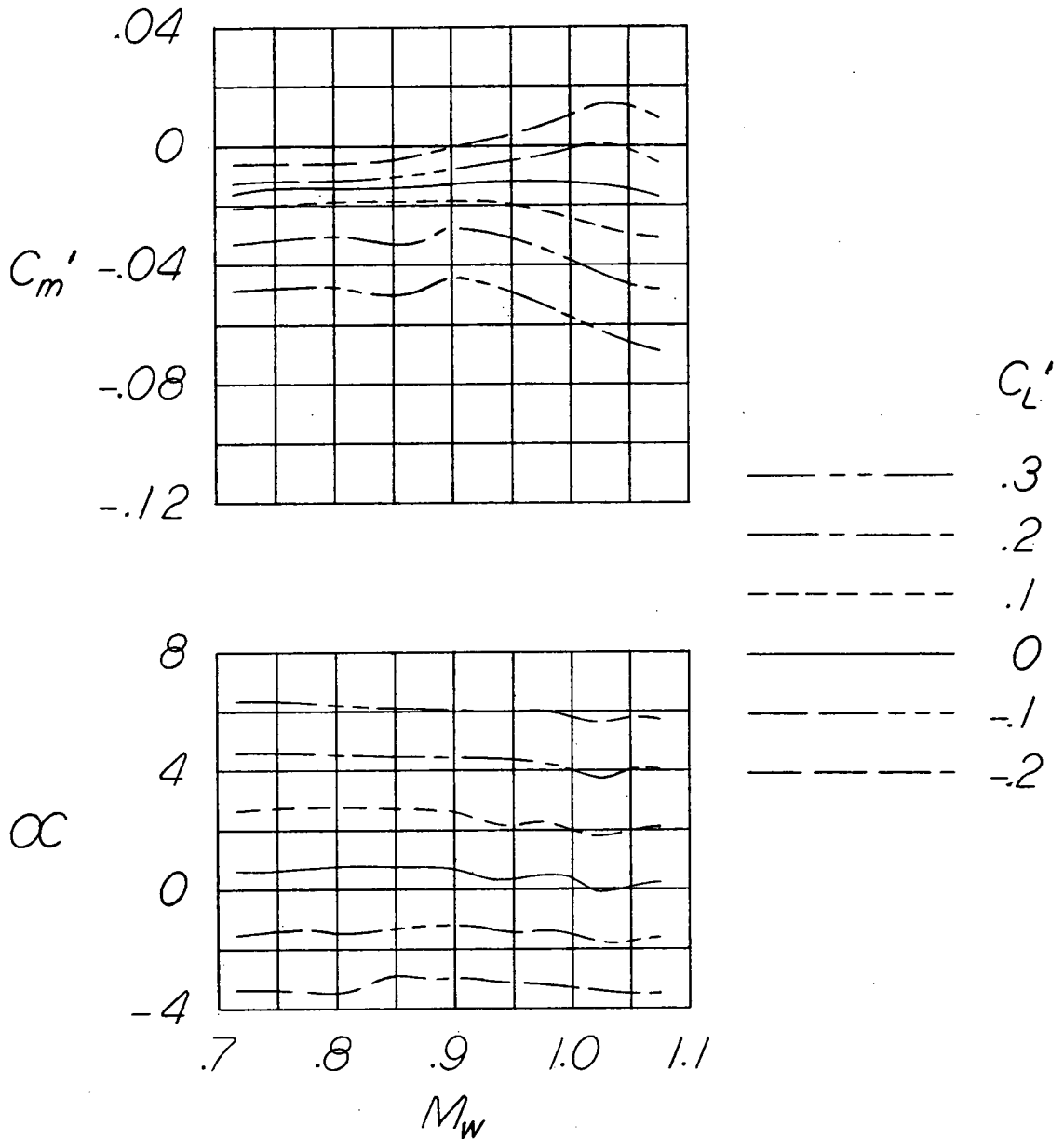
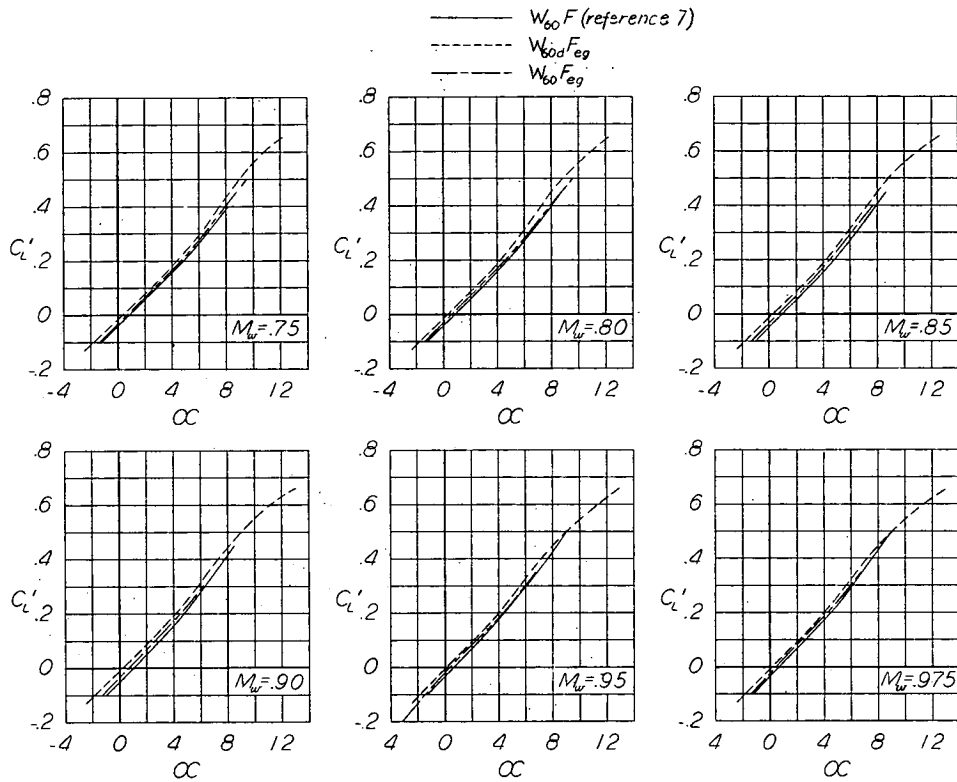
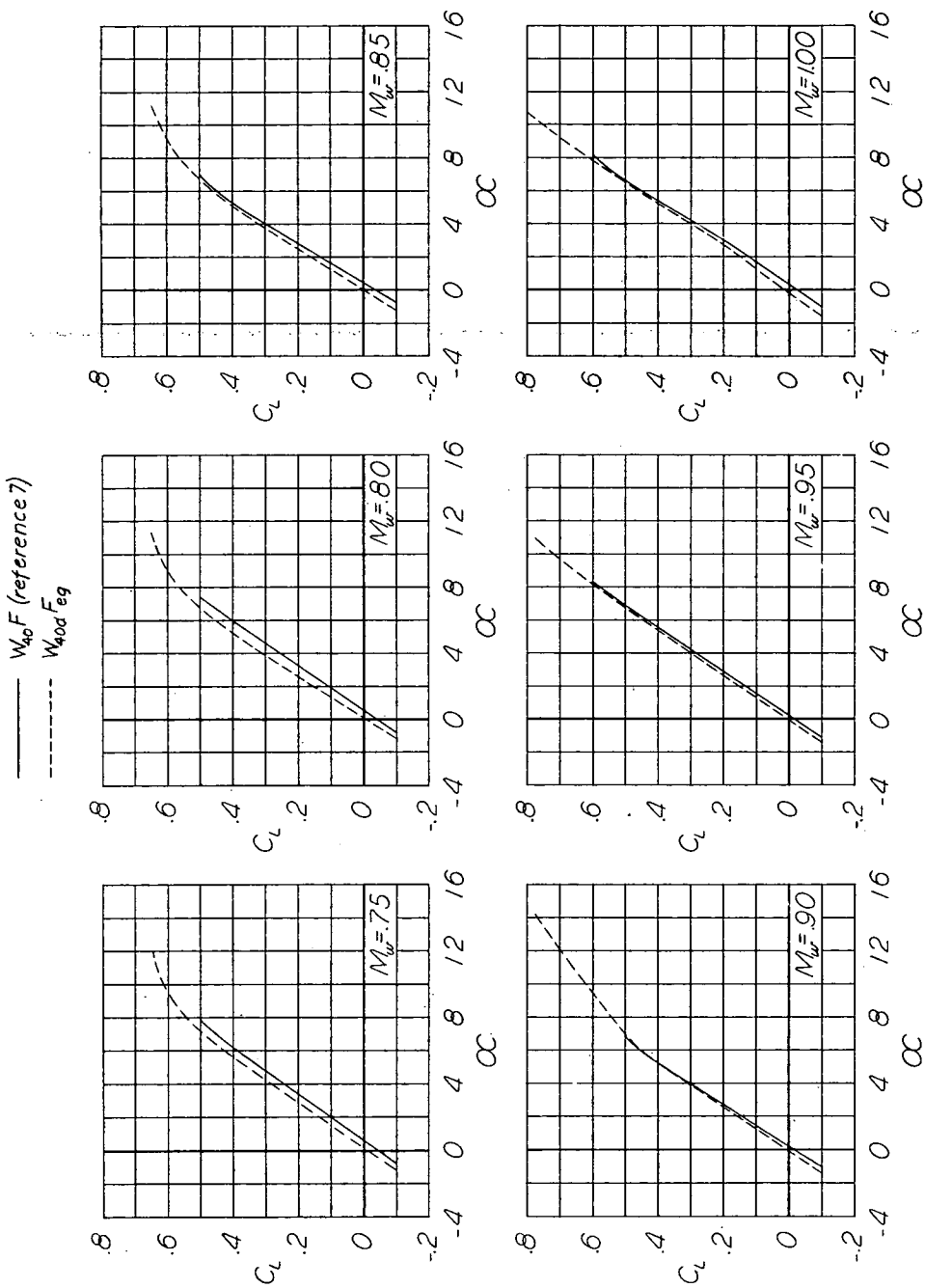


Figure 12.- Variation with Mach number of  $C_m'$  and  $\alpha$  at various lift coefficients for semispan wing-flow model of Bell X-5 airplane with  $60^\circ$  wing and end plate and gap of configurations  $W_{Ad}F_{eg}$  simulated. Configuration  $W_{60}F_{eg}$ ; tail off. (Coefficients based on  $60^\circ$  wing dimensions.)



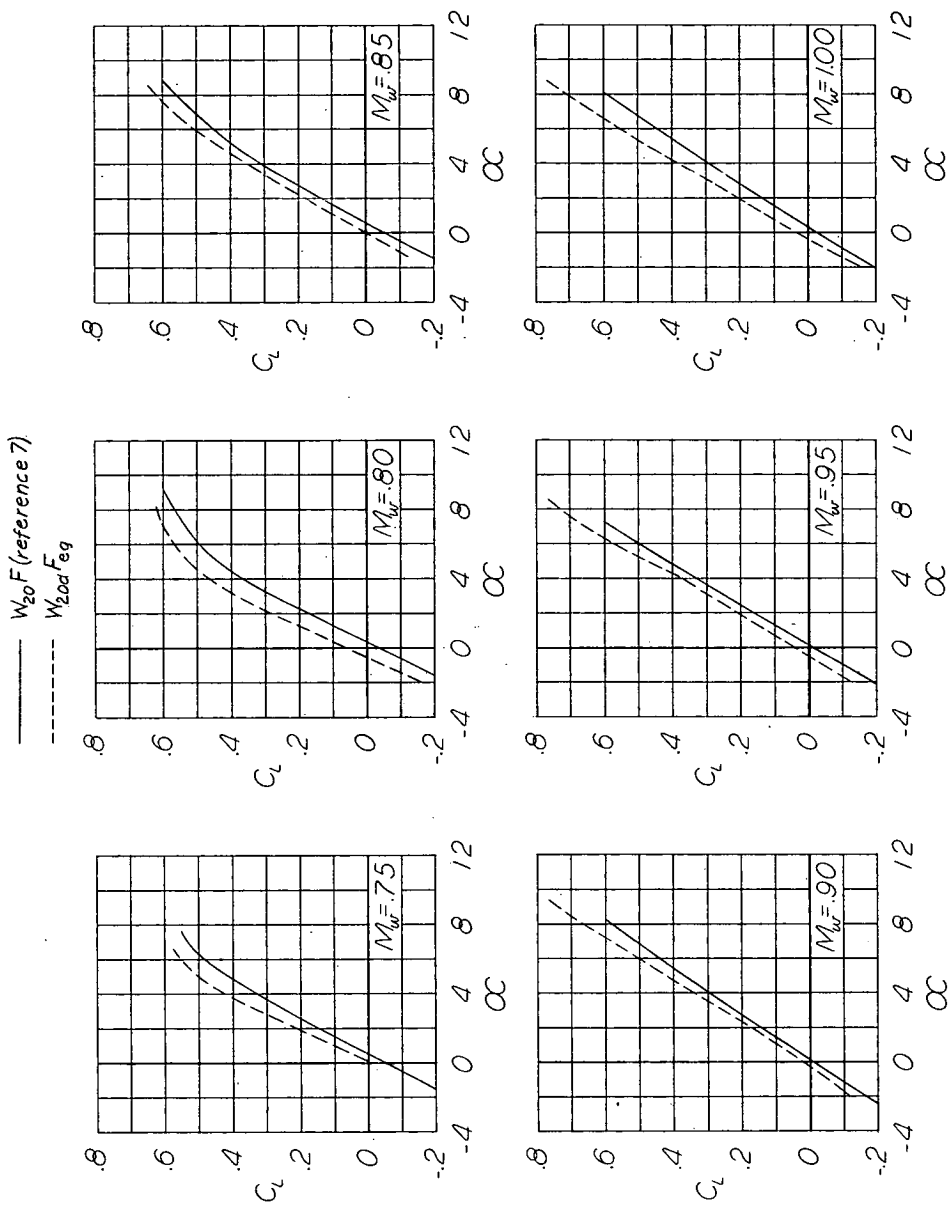
(a)  $\Lambda = 60^\circ$  ( $W_{60}F$ ,  $W_{60d}F_{eg}$ , and  $W_{60}F_{eg}$ ).

Figure 13.- Variation of  $C_L$  with  $\alpha$  for wing-detached configurations  $W_{Ad}F_{eg}$  and wing-fuselage configurations  $W_{\Lambda}F$  of reference 7 at various Mach numbers. Configuration  $W_{60}F_{eg}$  shown only for  $60^\circ$  sweep. Bell X-5 semispan wing-flow model; tail off. ( $C_L$  of configurations  $W_{Ad}F_{eg}$  based on respective exposed wing area;  $C_L$  of other configurations based on respective total wing area.)



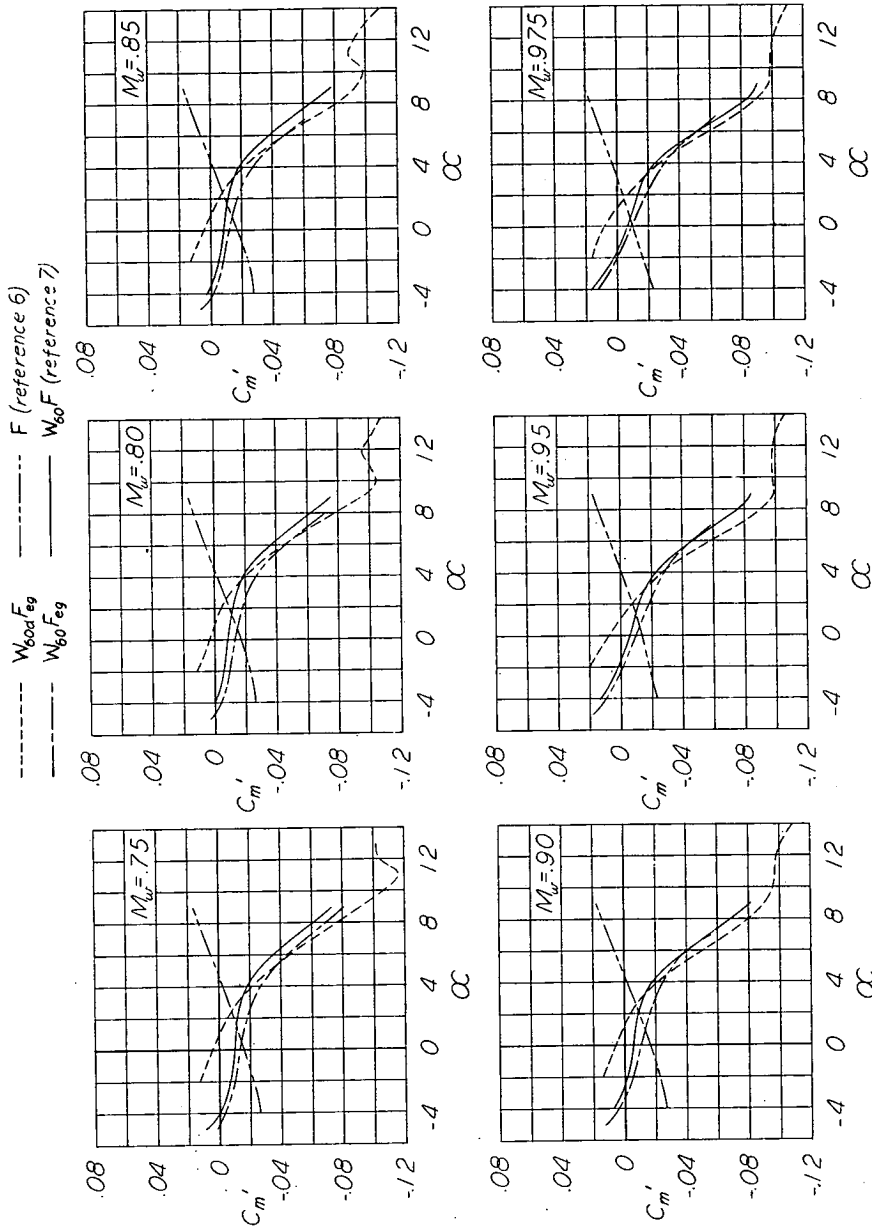
(b)  $\Lambda = 40^\circ$  ( $W_{40}F$  and  $W_{40d}F_{eg}$ ).

Figure 13.- Continued.



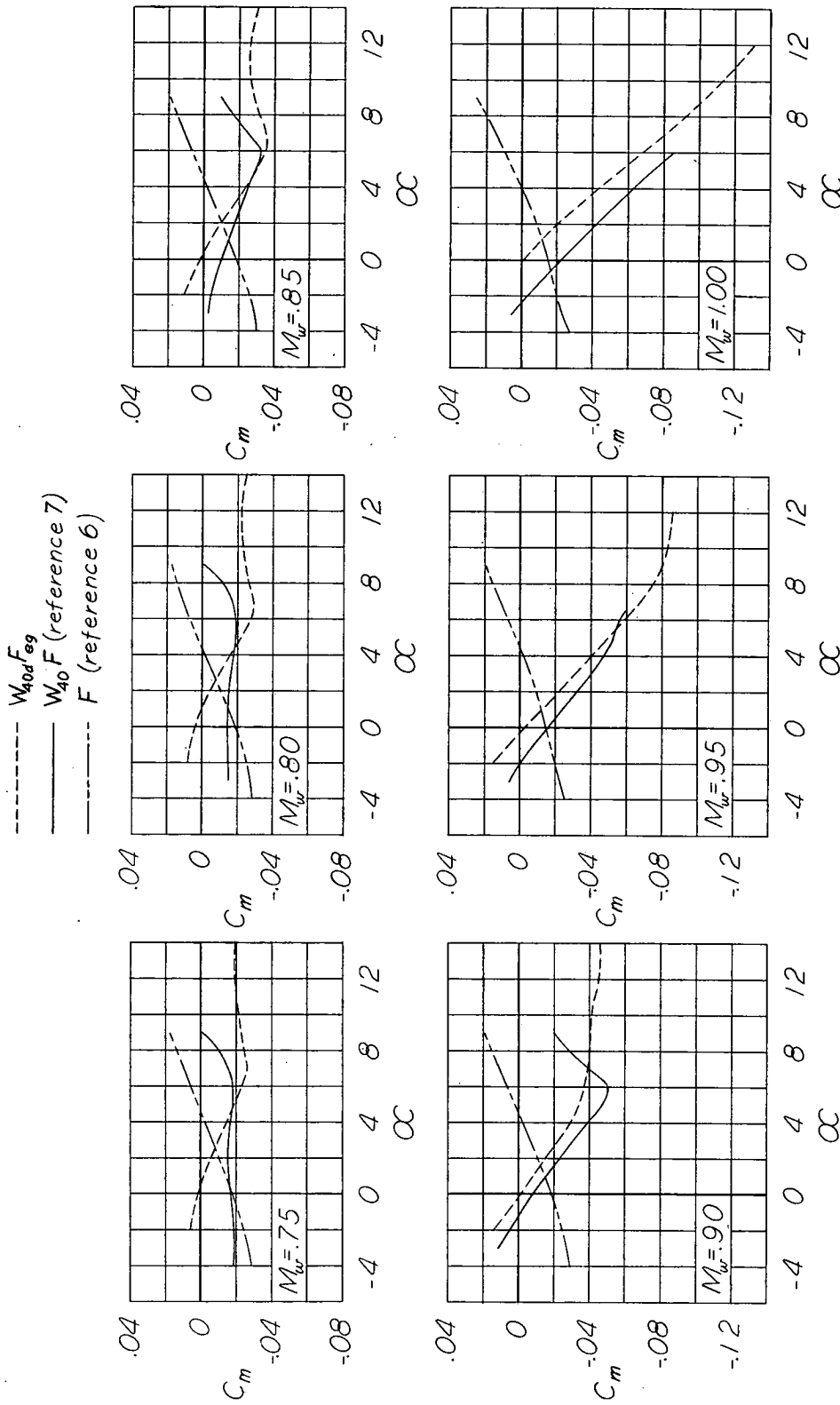
(c)  $\Lambda = 20^\circ$  ( $W_{20}F$  and  $W_{20d}F_{eg}$ ).

Figure 13.- Concluded.



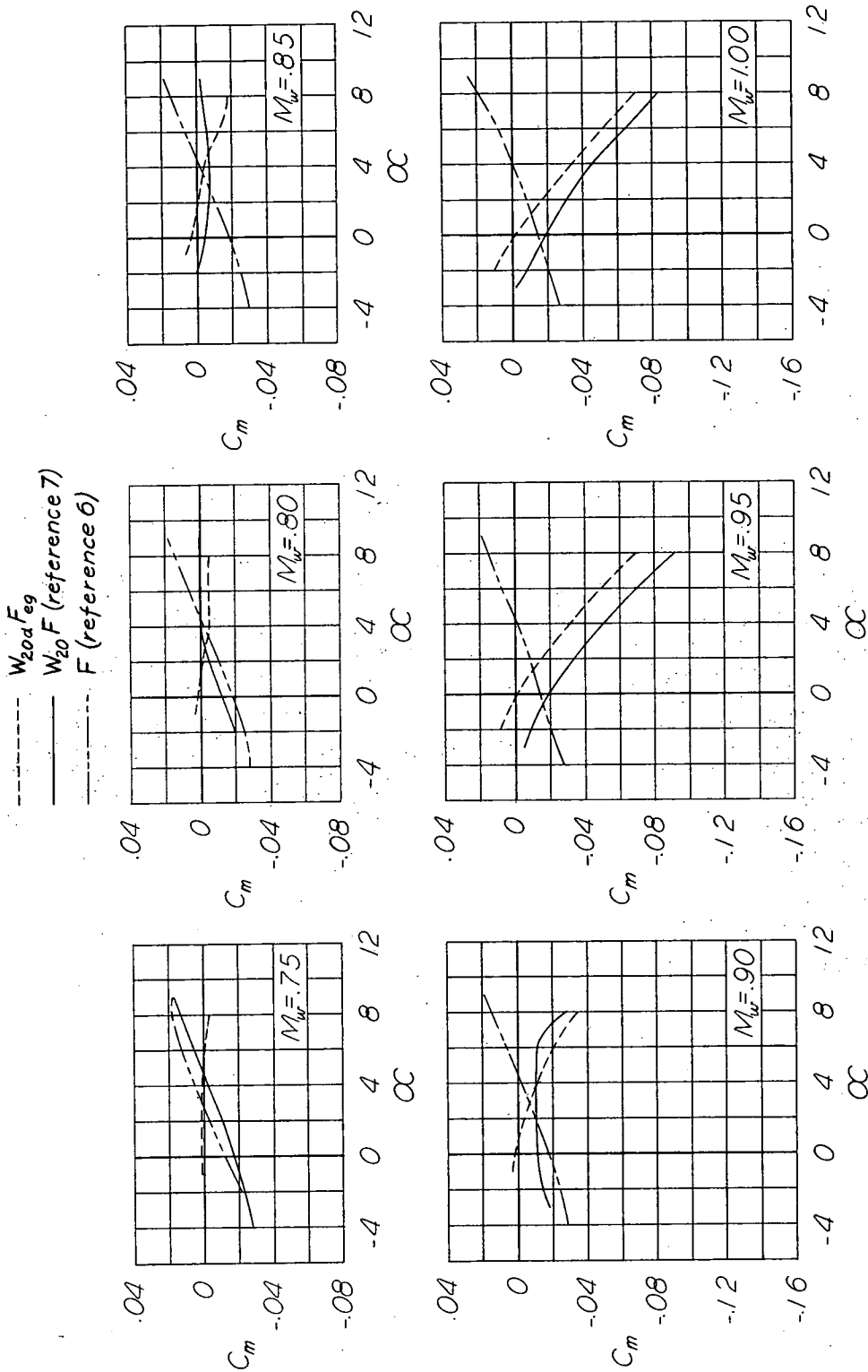
(a)  $\Lambda = 60^\circ$  ( $W_{60dFeg}$ ,  $W_{60Feg}$ ,  $F$ , and  $W_{60F}$ ).

Figure 14.- Variation of  $C_m$  with  $\alpha$  for wing-detached configurations  $W_{\Lambda dFeg}$ , simulated gap configuration  $W_{60Feg}$ , and fuselage  $F$  and wing-fuselage configurations  $W_{\Lambda F}$  of references 6 and 7, respectively. Bell X-5 semispan airplane model.



(b)  $\Lambda = 40^\circ$  ( $W_{40d}F_{eg}$ ,  $F$ , and  $W_{40}F$ ).

Figure 14.- Continued.



(c)  $\Lambda = 20^\circ$  ( $W_{20d}F_{eg}$ ,  $W_{20}F$ , and  $F$ ).

Figure 14.- Concluded.

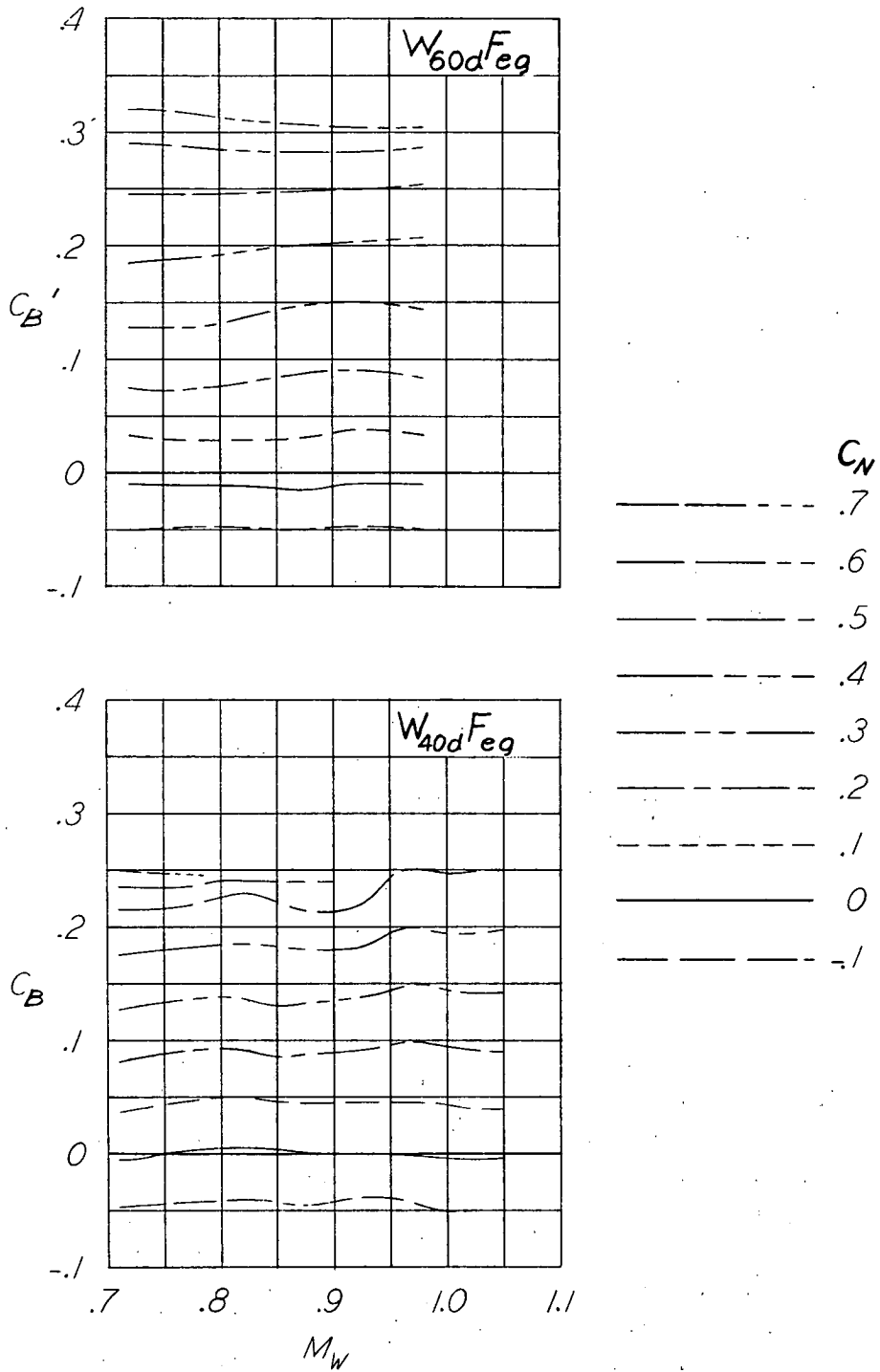


Figure 15.- Variation with Mach number of bending-moment coefficient referred to the wing pivot point for various normal force coefficients for configurations  $W_{60dFeg}$  and  $W_{40dFeg}$ . (Coefficients based on respective exposed-wing dimensions.)

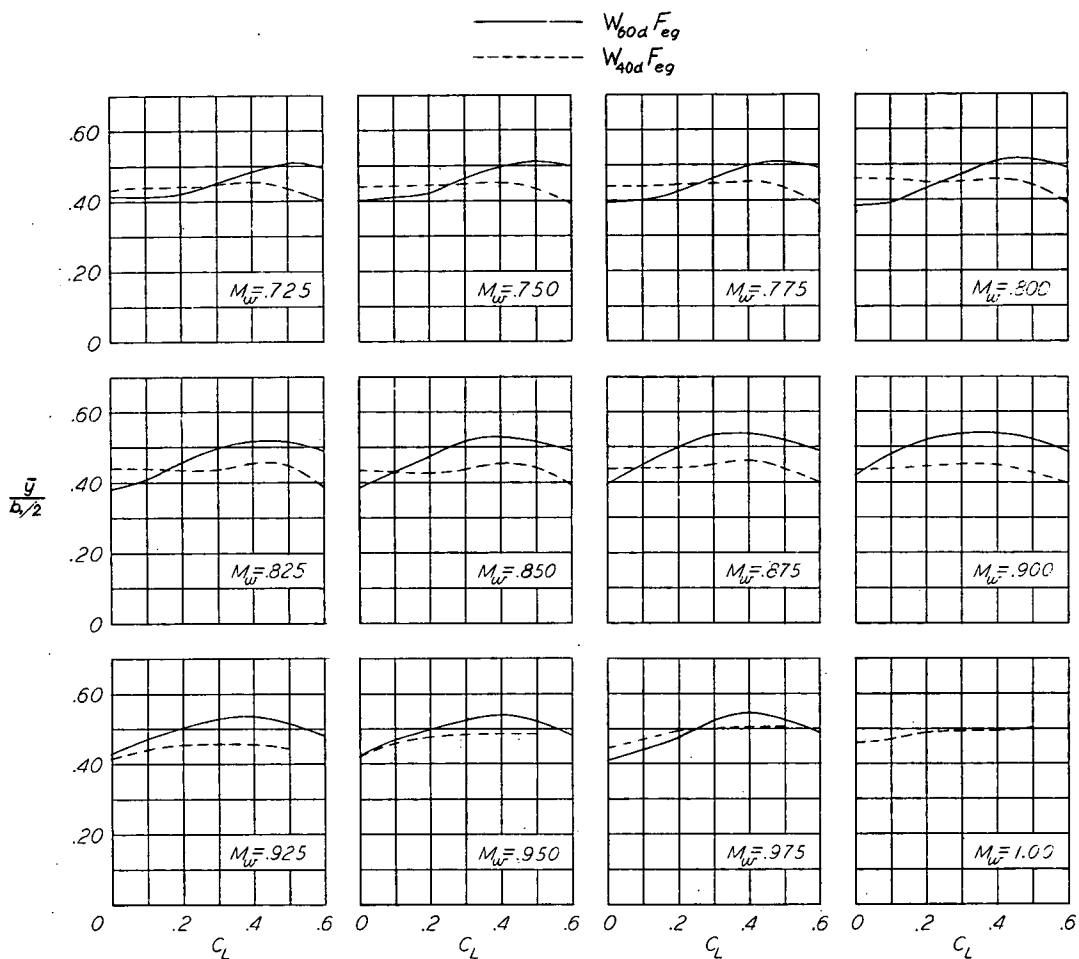


Figure 16.- Variation with lift coefficient of spanwise center-of-pressure location outboard of pivot point for configurations  $W_{60d}F_{eg}$  and  $W_{40d}F_{eg}$ . Bell X-5 semispan airplane model. (Coefficients based on respective exposed wing areas.)

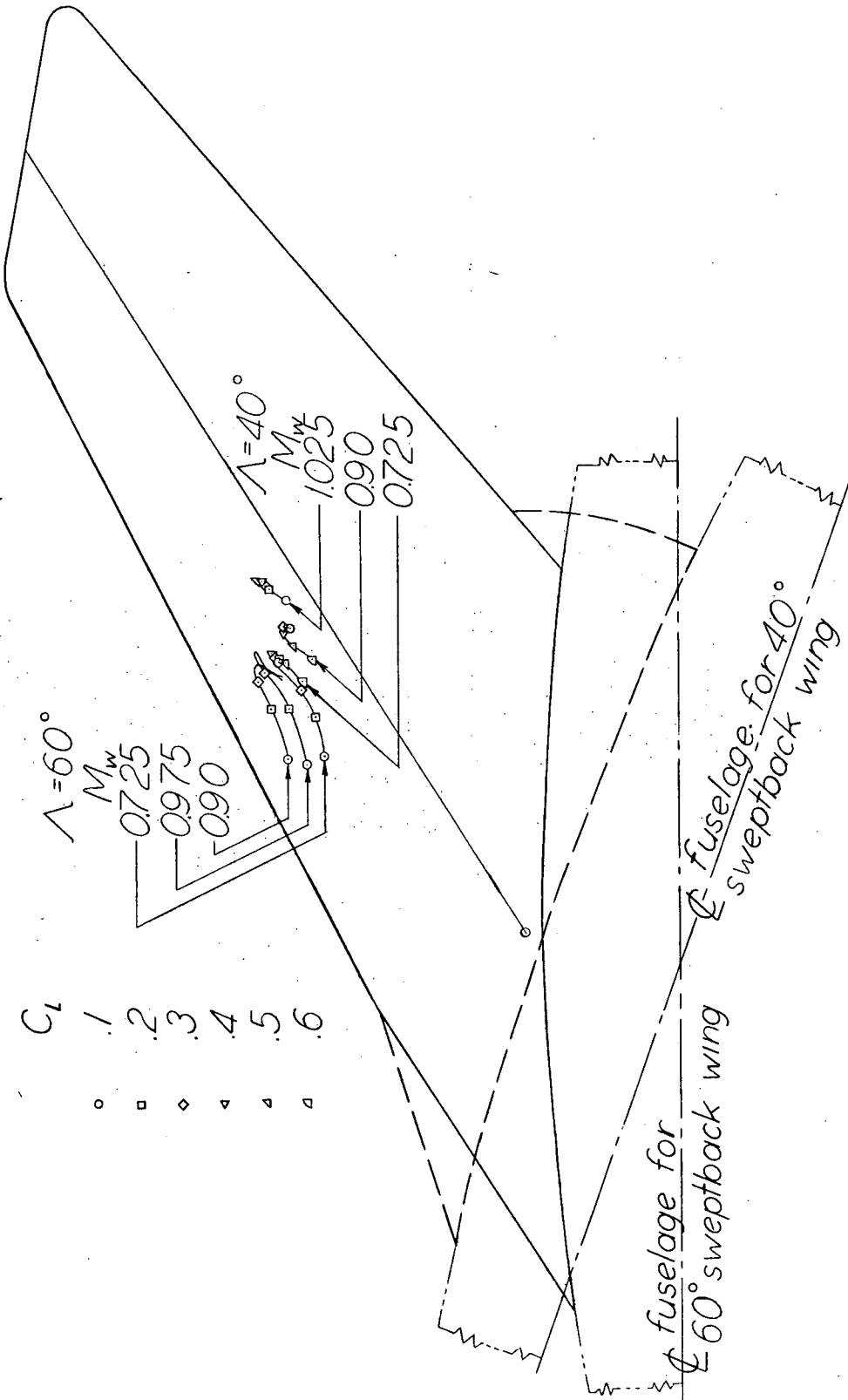


Figure 17.- Center-of-pressure location on exposed wings at various lift coefficients and Mach numbers for configurations W60dFeg and W40dFeg. (Coefficients based on respective exposed-wing dimensions.)

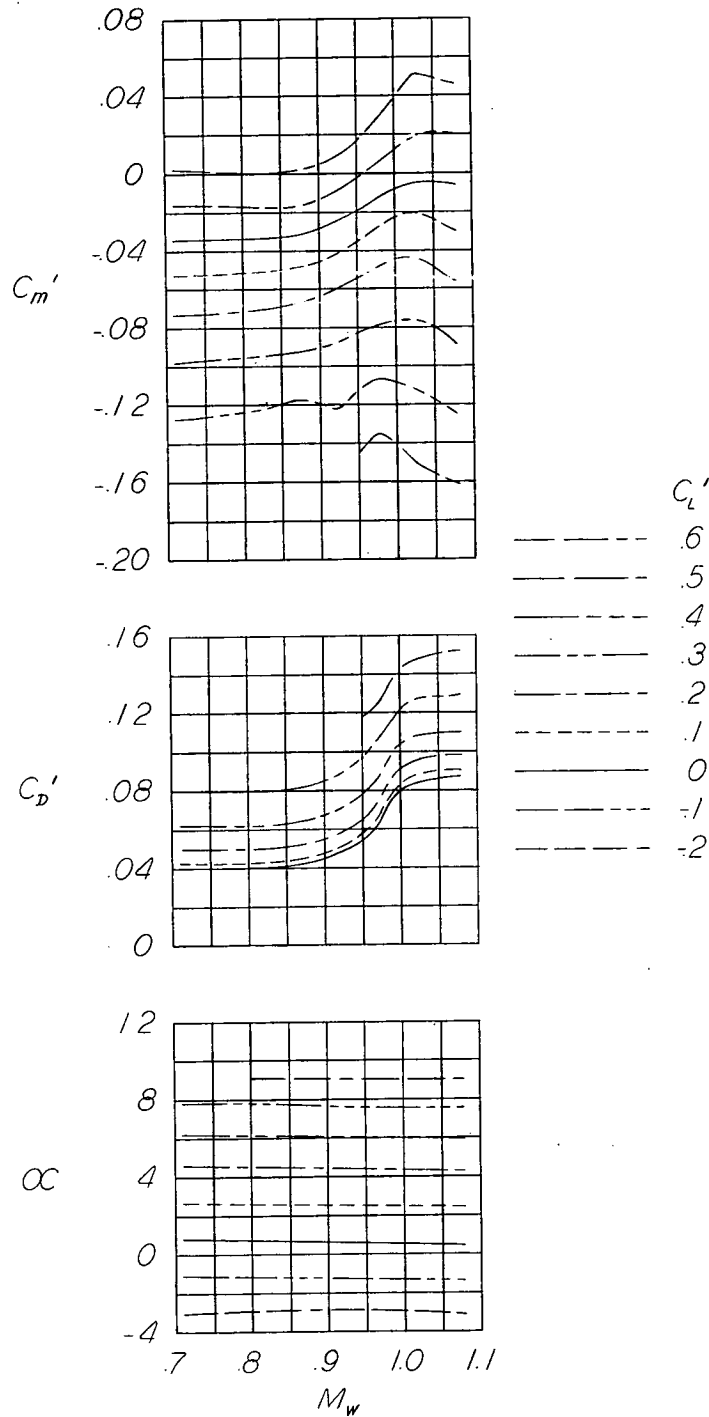
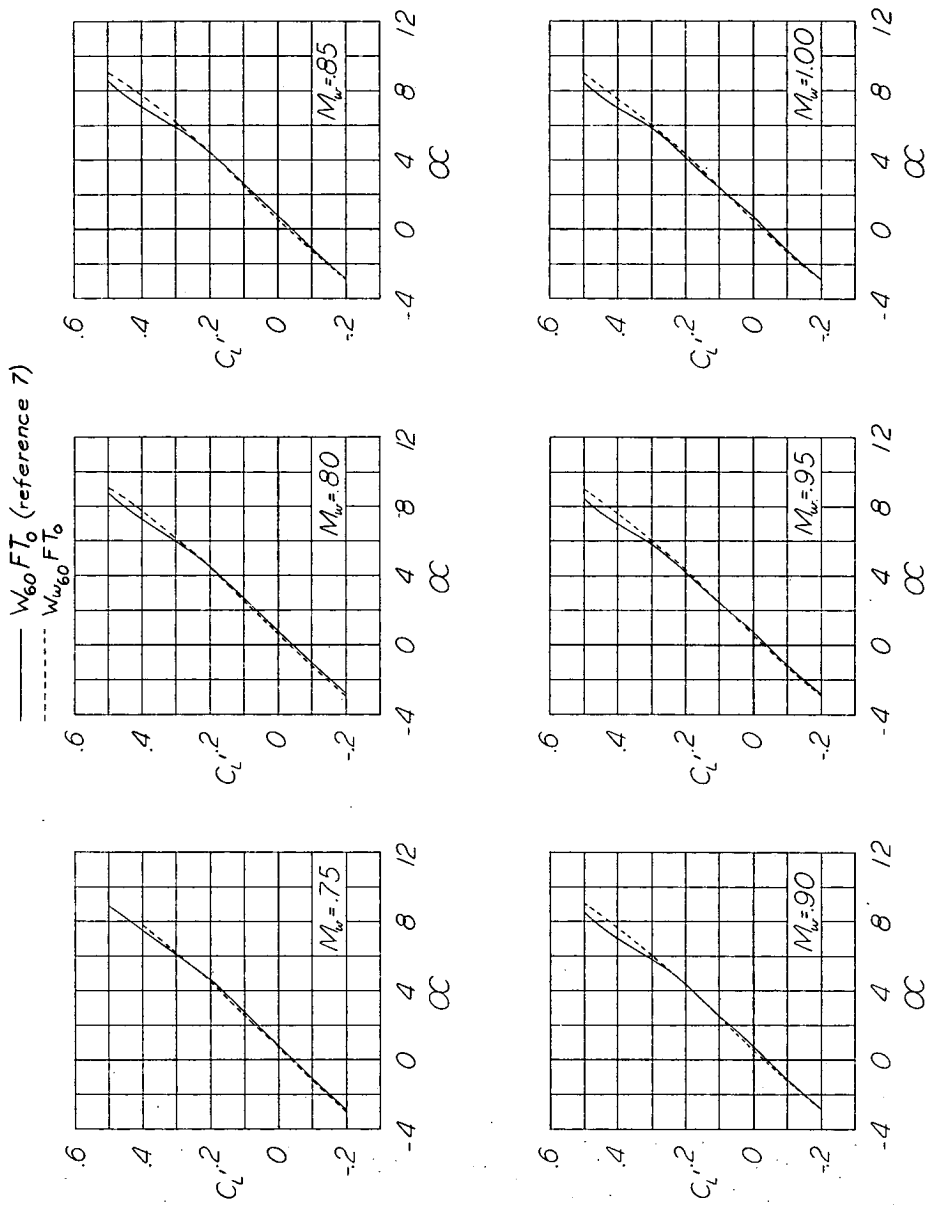
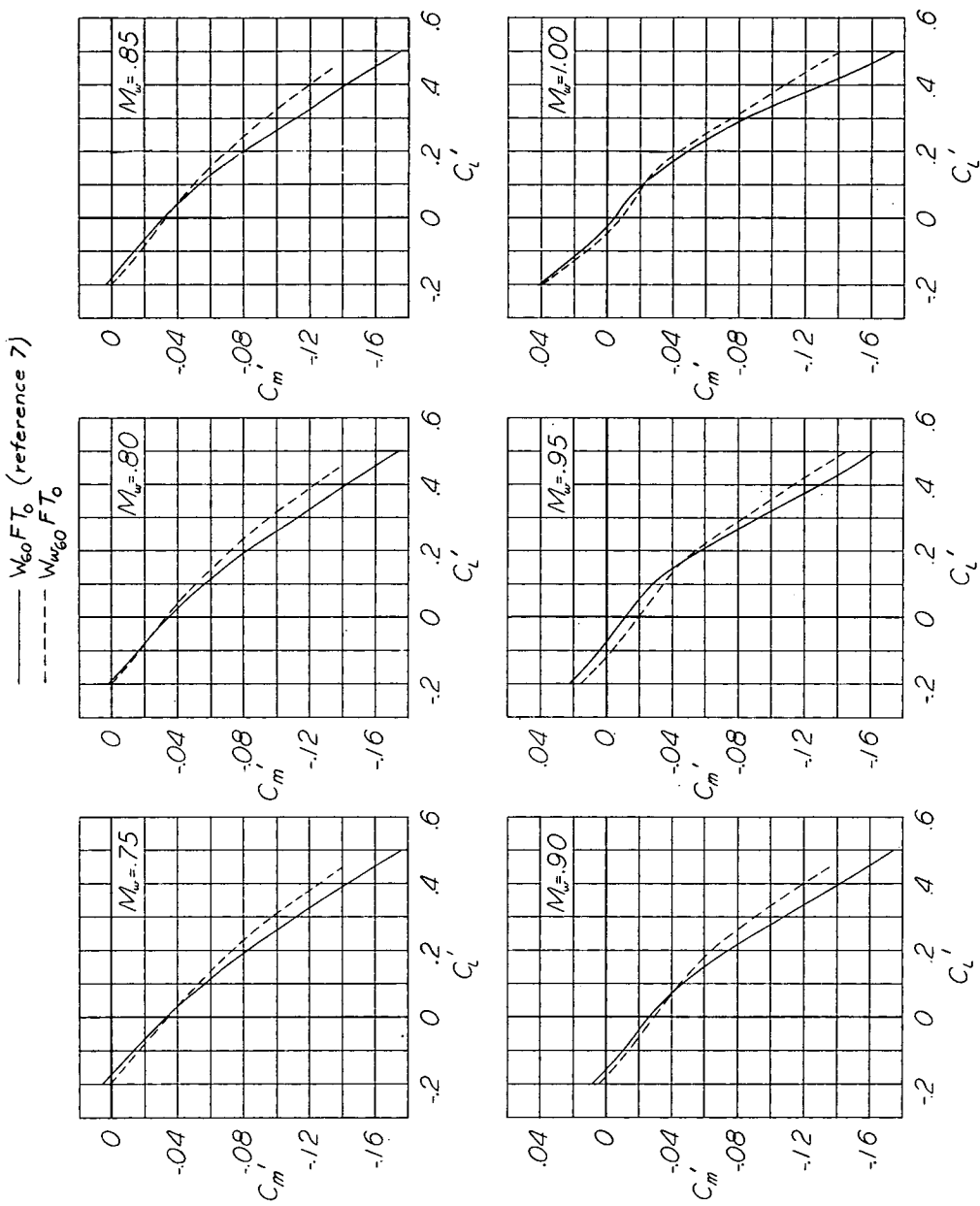


Figure 18.- Variation with Mach number of  $C_m'$ ,  $C_D'$ , and  $\alpha$  at various lift coefficients for configuration  $W_{w60}^{FT0}$ . Bell X-5 semispan airplane model. (Coefficients based on  $60^\circ$  sweptback-wing dimensions.)



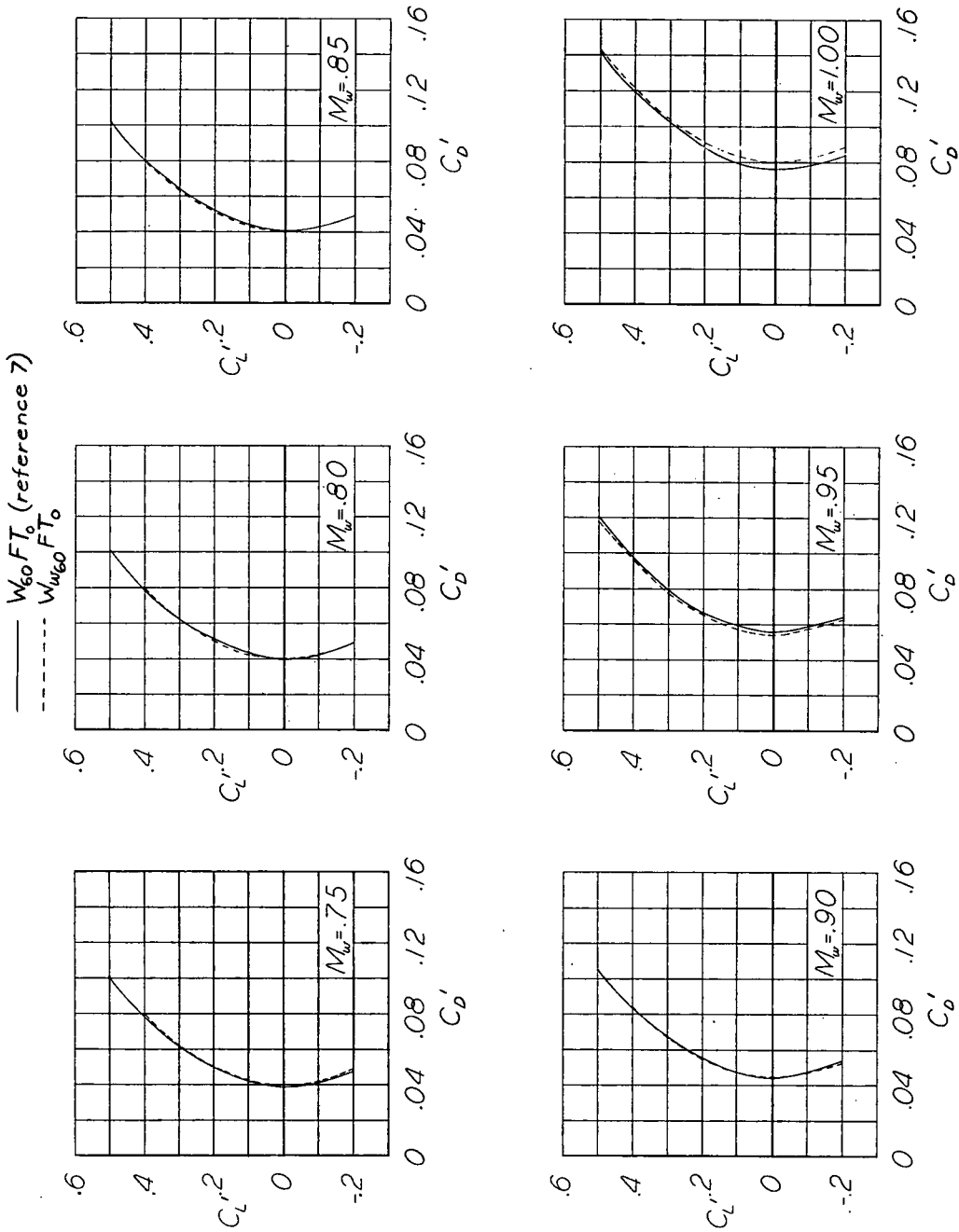
(a)  $C_L'$  against  $\alpha$ .

Figure 19.- Comparison of aerodynamic characteristics of configurations  $W_{60} F_{T_0}$  and  $W_{w60} F_{T_0}$ . Bell X-5 semispan airplane model. (Coefficients based on  $60^\circ$  sweptback-wing dimensions.)



(b)  $C_m'$  against  $C_l'$ .

Figure 19.- Continued.



(c)  $C_L'$  against  $C_D'$ .

Figure 19.- Concluded.

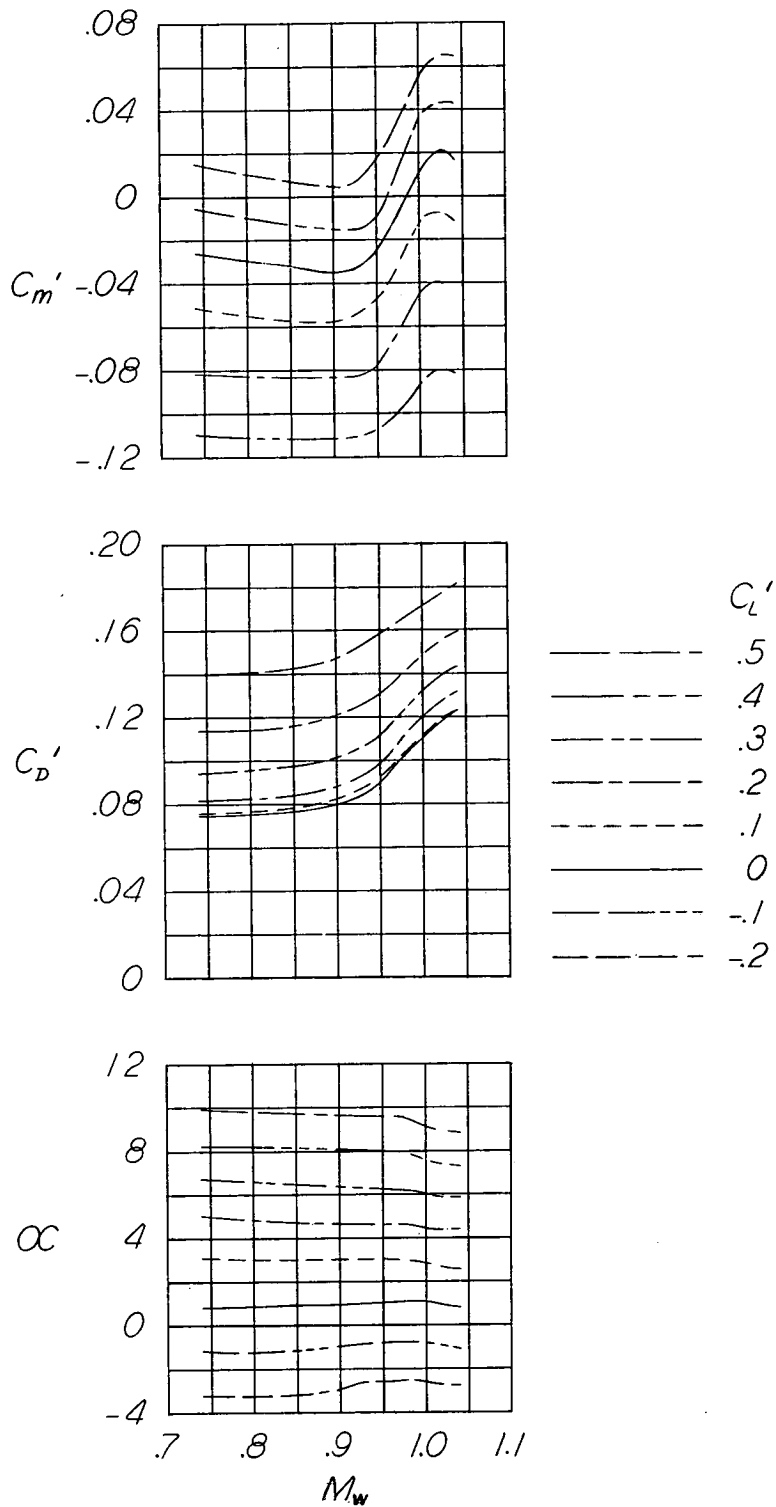
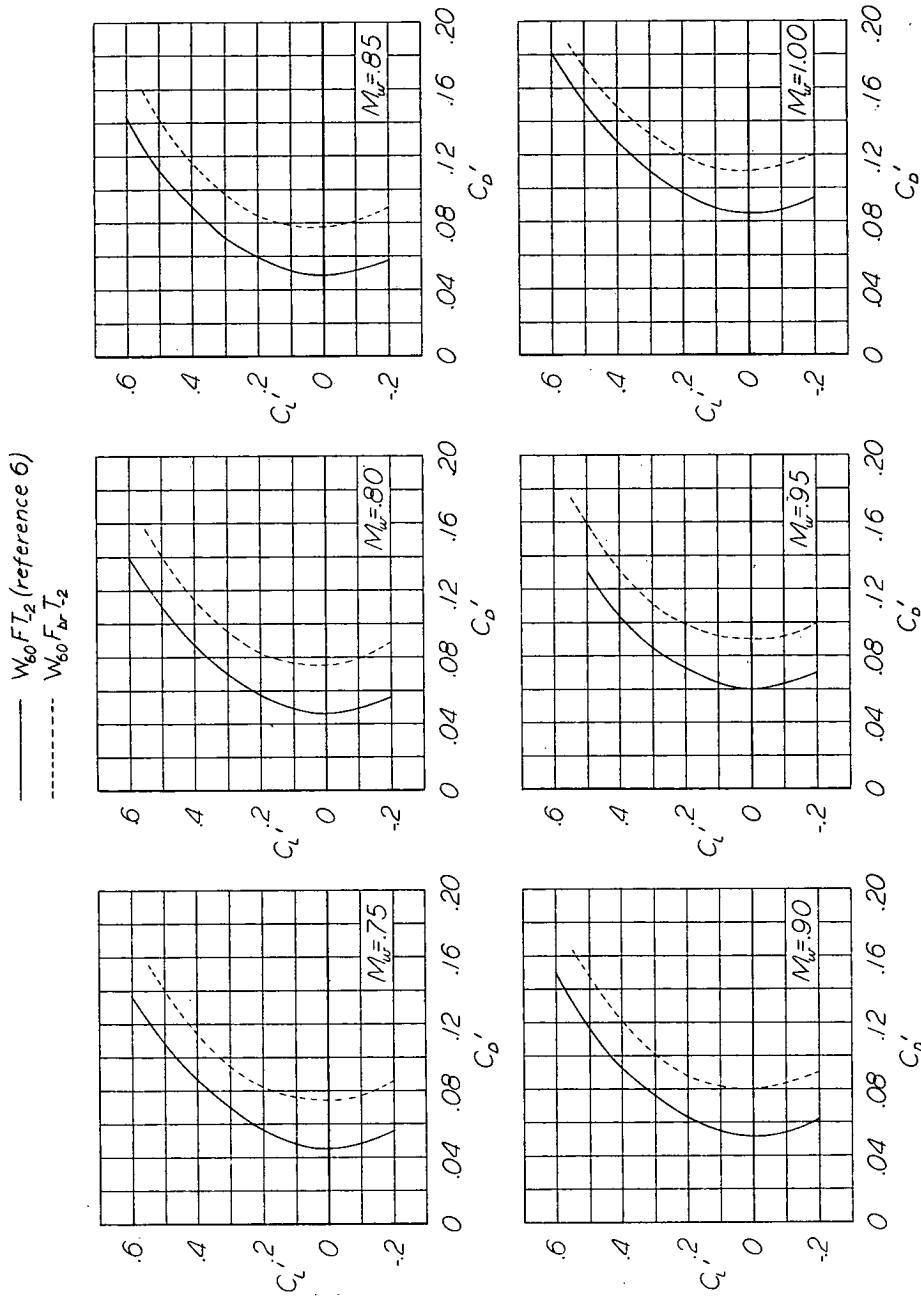
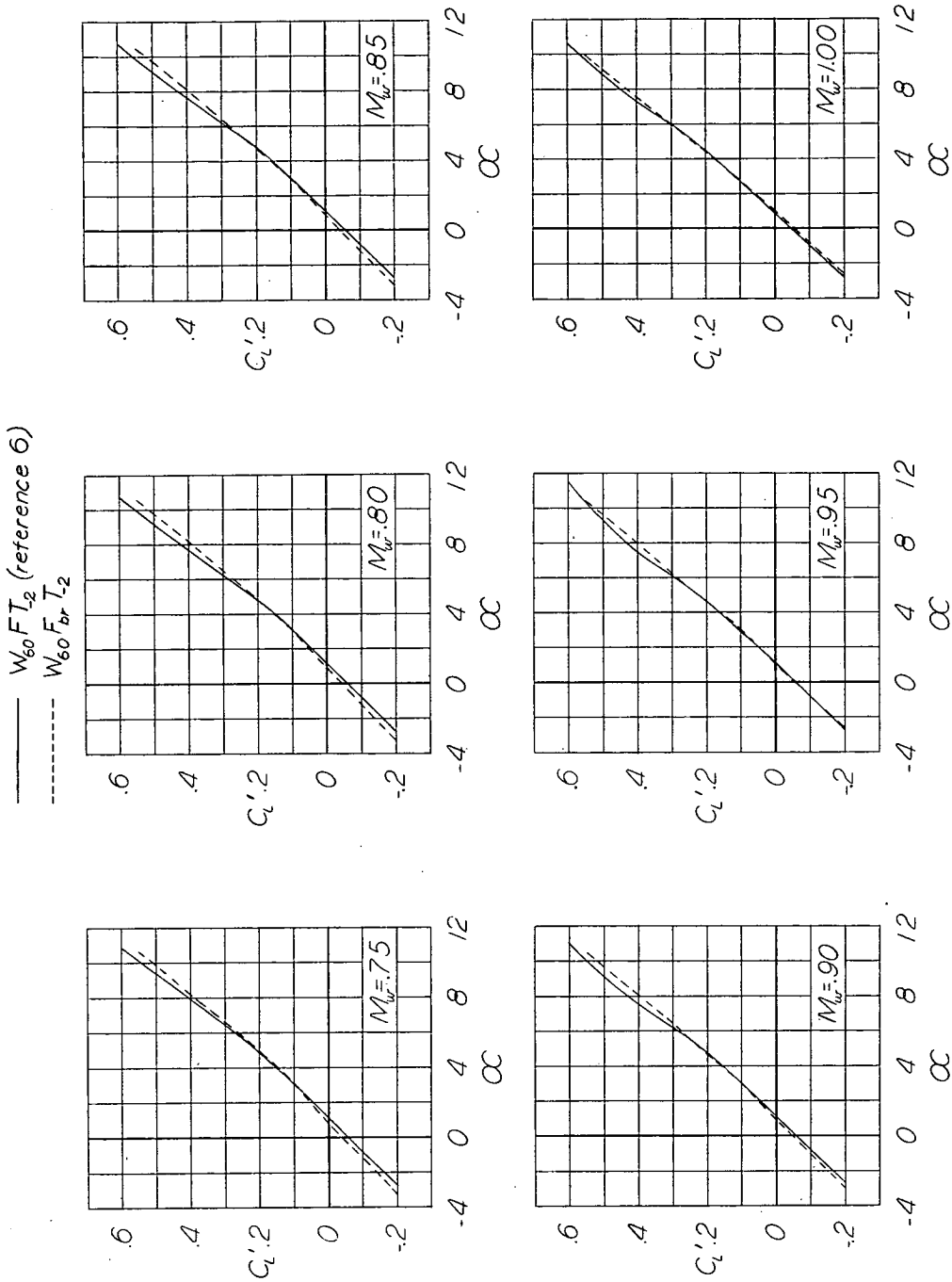


Figure 20.- Variation with Mach number of  $C_m'$ ,  $C_D'$ , and  $\alpha$  at various lift coefficients for configuration  $W_{60}F_{br}T-2$ . Bell X-5 semispan airplane model.



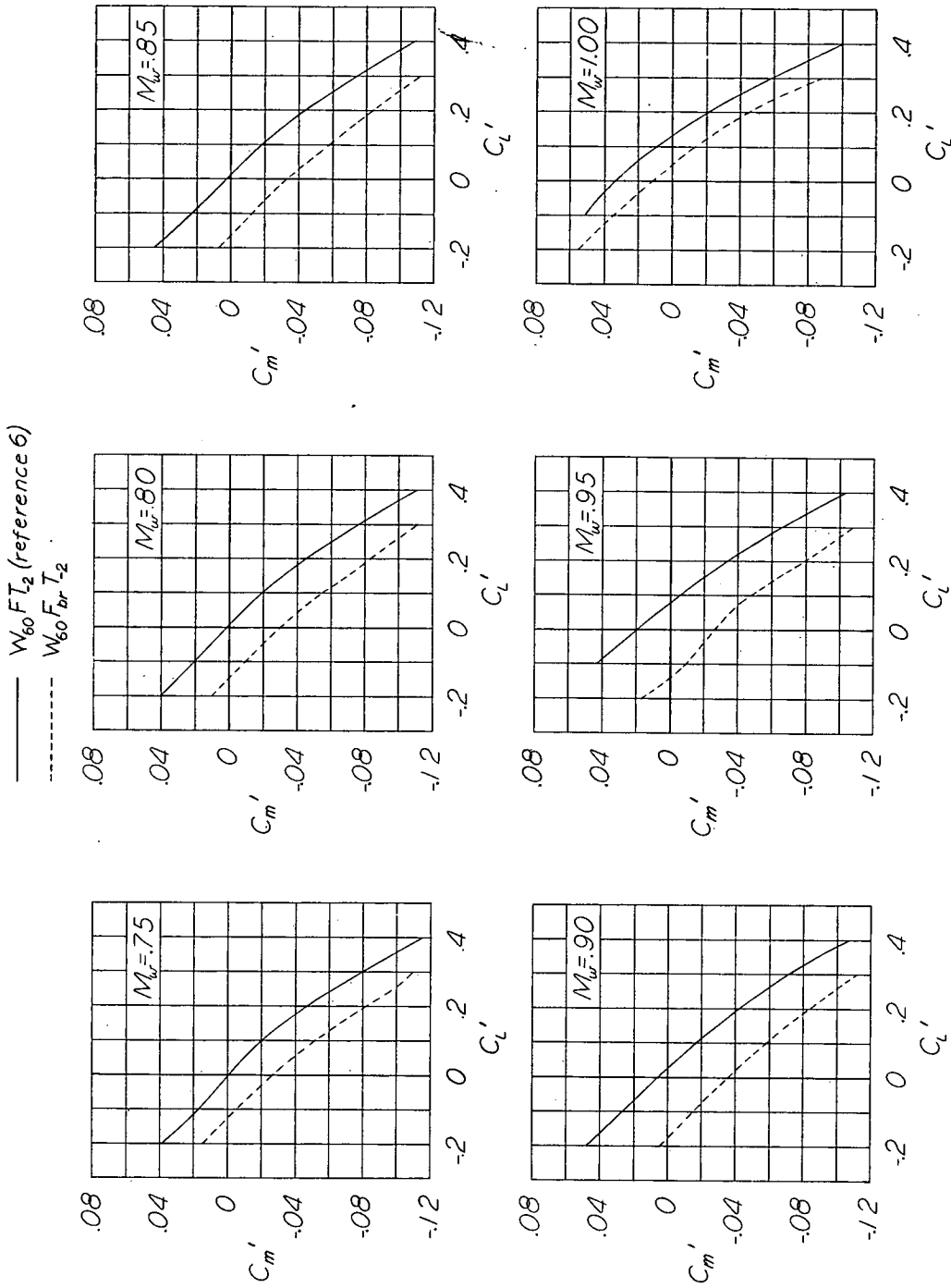
(a)  $C_L'$  against  $C_D'$ .

Figure 21.- Comparison of the aerodynamic characteristics of configurations  $W_{60}F_{brT-2}$  and  $W_{60}FT-2$ . Bell X-5 semispan airplane model. (Coefficients based on  $60^\circ$  sweptback wing dimensions.)



(b)  $C_L'$  against  $\alpha$ .

Figure 21.- Continued.



(c)  $C_m'$  against  $C_L'$ .

Figure 21.- Concluded.

CONFIDENTIAL

CONFIDENTIAL